



JGR Earth Surface

RESEARCH ARTICLE

10.1029/2023JF007255

Kev Points:

- Increased runoff drives increased solute export in glacierized catchments
- The hydrologic and landscape changes associated with deglaciation modifies the weathering CO₂ balance of catchments
- Weathering flux estimates that do not account for dilution overestimate contributions in glacierized catchments

Supporting Information:

Supporting Information may be found in the online version of this article.

Correspondence to:

S. Muñoz, sebastian_munoz@brown.edu

Citation:

Muñoz, S., Jenckes, J., Ramos, E. J., Munk, L. A., & Ibarra, D. E. (2024). Hydrologic and landscape controls on rock weathering along a glacial gradient in South Central Alaska, USA. *Journal* of *Geophysical Research: Earth Surface*, 129, e2023JF007255. https://doi. org/10.1029/2023JF007255

Received 12 MAY 2023 Accepted 22 JAN 2024

Hydrologic and Landscape Controls on Rock Weathering Along a Glacial Gradient in South Central Alaska, USA

S. Muñoz^{1,2} D, J. Jenckes^{3,4} D, E. J. Ramos^{1,5} D, L. A. Munk³ D, and D. E. Ibarra^{1,2} D

¹Department of Earth, Environmental and Planetary Sciences, Brown University, Providence, RI, USA, ²Institute at Brown for Environment and Society, Brown University, Providence, RI, USA, ³Department of Geological Sciences, University of Alaska Anchorage, Anchorage, AK, USA, ⁴Department of Geosciences, University of Alaska Fairbanks, Fairbanks, AK, USA, ⁵Department of Earth, Environmental, and Planetary Sciences, Rice University, Houston, TX, USA

Abstract Rock weathering impacts atmospheric CO₂ levels with silicate rock dissolution removing CO₂ and carbonate dissolution, pyrite oxidation, and organic rock carbon oxidation producing CO₂. Glacierization impacts the hydrology and geomorphology of catchments and glacier retreat due to warming can increase runoff and initiate landscape succession. To investigate the impact of these changes on catchment scale weathering CO₂ balances, we report monthly samples of solute chemistry and continuous discharge records for a sequence of glacierized watersheds draining into Kachemak Bay, Alaska. We partition solute and acid sources and estimate inorganic weathering CO₂ balances using an inverse geochemical mixing model. Furthermore, we investigated how solutes vary with discharge conditions utilizing a concentration-runoff framework. We develop an analogous fraction-runoff framework which allows us to investigate changes in weathering contributions at different flows. Fraction-runoff relationships suggest kinetic limitations on all reactions in glacierized catchments, and only silicate weathering in less glacierized catchments. Using forest cover as a proxy for landscape age and stability, multiple linear regression shows that faster reactions (pyrite oxidation) contribute less to the solute load with increasing forest cover, whereas silicate weathering (slow reaction kinetics) contributes more. Overall, in glacierized catchments, we find elevated weathering fluxes at high runoff despite significant dilution effects. This makes flux estimates that account for dilution more important in glacierized catchments. Our findings quantify how glaciers modify the inorganic weathering CO₂ balance of catchments through hydrologic and geomorphic forcings, and support the previous hypothesis that deglaciation will be accompanied by a shift in inorganic weathering CO₂ balances.

Plain Language Summary The chemical breakdown of rocks impacts atmospheric CO₂ levels and helps regulate Earth's climate. The concentration of elements in river water reflects the chemical reactions occurring across a watershed, and the number of glaciers on the landscape can impact the breakdown of rocks. To understand the influence glaciers have on the chemical breakdown of rocks and how that influences CO₂ balances, we collected water monthly from 5 rivers that drain landscapes with varying number of glaciers. We utilize a mixing model to understand which reactions are taking place in each watershed, quantify the CO₂ balances associated with the chemical breakdown of rocks and develop a framework for understanding how these reactions change with changing hydrologic conditions. Watersheds with more glaciers have greater chemical breakdown of rocks, even though element concentrations in rivers are lower. Accounting for this dilution is more important in watersheds with high amounts of glacier cover. Additionally, in watersheds with higher glacier cover, all rock water reactions are limited by the time water is in contact with reactive minerals. This work suggests that glacier retreat will impact the balance of CO₂ in the atmosphere because of the way glaciers impact the way rocks break down.

1. Introduction

Earth's habitability relies on self-regulating systems (or feedback loops) that maintain surface conditions within the window which has allowed life to develop and thrive (Kasting & Catling, 2003; Loper, 2009; Nicholson, 2019). Atmospheric concentrations of CO₂ impact the hydrology (Gleick, 1987; Idso et al., 1990; Salmon-Monviola et al., 2013; Schäfer et al., 2002) and energy budget (Pittock & Salinger, 1982; Schneider, 1984) of the Earth's surface, the acidity of the ocean (IPCC, 2014; Raven et al., 2005), and nearly all life on Earth. The seminal work of researchers in the 1980s (Berner et al., 1983; Lovelock & Watson, 1982; Walker et al., 1981; Watson & Lovelock, 1983) proposed that the weathering of rocks stabilized Earth's temperature and climate over geologic

© 2024. American Geophysical Union. All Rights Reserved.

MUÑOZ ET AL. 1 of 24

time. The mechanism proposed by their hypotheses relies on the dissolution and breakdown of rocks (e.g., silicate weathering). In general, these reactions produce alkalinity (HCO₃⁻), cations (Ca²⁺, Mg²⁺, K⁺, Na⁺), and silica that are transported through rivers to the ocean and serve as a long-term geologic sink of carbon through the deposition of Ca and Mg bearing carbonates (Equations 1 and 2).

$$2CO_2 + 3H_2O + CaAl_2Si_2O_8 \rightarrow Ca^{2+} + 2HCO_3^- + Al_2Si_2O_5(OH)_4$$
 (1)

$$Ca^{2+} + 2HCO_3^- \rightarrow CaCO_3 + CO_2 + H_2O$$
 (2)

This process responds to global temperature, hydrologic intensity, and atmospheric partial pressures of CO₂ and serves as dampening feedback on the earth's climate (Berner et al., 1983; Lovelock & Watson, 1982; Walker et al., 1981; Watson & Lovelock, 1983). Additional work has demonstrated that tectonic and hydrologic factors modify the strength of the feedback, with mountains amplifying the hydrologic cycle and determining the availability of mineral surfaces for dissolution (Gaillardet et al., 1999; Maher, 2011; Maher & Chamberlain, 2014; Millot et al., 2003; Stallard, 1998; West et al., 2005). However, recently attention has been drawn to the oxidation of pyrite and dissolution of carbonates which may counteract the silicate weathering feedback due to rapid reaction kinetics and the release of CO₂ (Bufe et al., 2021; Burke et al., 2018; Calmels et al., 2007; Hilton & West, 2020; Kemeny et al., 2021; Torres et al., 2014, 2016). The reaction of these minerals is facilitated by their co-occurrence in metasedimentary and sedimentary lithologies of oceanic origin and is primarily influenced by erosion creating exposure to oxidizing conditions (Hilton & West, 2020). Although here we focus on inorganic rock weathering reactions, we note that the organic carbon sub-cycle of burial and oxidation responds to these forcings as well (for more discussion see Hilton & West, 2020; Horan et al., 2017). To illustrate the influence of pyrite oxidation and carbonate dissolution we include Equations 3–5 from Hilton and West (2020) that show the pairing of carbonate dissolution with pyrite oxidation resulting in a potential source of CO₂.

$$CaCO_3 + CO_2 + H_2O \rightarrow Ca^{2+} + 2HCO_3^-$$
 (3)

$$4\text{FeS}_2 + 15\text{O}_2 + 14\text{H}_2\text{O} \rightarrow 4\text{Fe}(\text{OH})_3 + 8\text{H}_2\text{SO}_4$$
 (4)

$$CaCO_3 + H_2SO_4 \rightarrow Ca^{2+} + CO_2 + H_2O + SO_4^{2-}$$
 (5)

Taken together, this demonstrates that multiple weathering reactions determine the long-term CO₂ budget in the ocean-atmosphere system and that hydrologic and landscape factors (erosion, landscape age) as well as mineral availability set by lithology are fundamental factors that regulate rock weathering. Except for lithology, glacierization modifies all of these factors and thus potentially influences the weathering reactions that dampen fluctuations in earth's climate.

Mountain glaciers impact watershed hydrology by modifying the supply of water (Immerzeel et al., 2010), the timing of peak runoff (Jansson et al., 2003) and influencing both riverine and coastal water quality (Hood et al., 2015; Jenckes et al., 2022, 2023). They store water on short and long time scales and have the capacity to decrease or increase runoff depending on their long-term mass gain or loss (Jansson et al., 2003). The storage capacity of glaciers results in a buffering effect where discharge fluctuations in glacierized systems are less than those in snowmelt- or rain-dominated systems (Fountain & Tangborn, 1985; Jansson et al., 2003; Pritchard, 2017). These attributes underscore glaciers as a reliable water resource, and over 1.9 billion people worldwide depend on streamflow generated from glacierized high mountains (Viviroli et al., 2011). Studies of modern glacial extent have shown accelerating declines in ice cover from warming which has increased melt contributions and produced elevated runoff in streams which will likely peak and then subside before 2100 (Bliss et al., 2014; Huss & Hock, 2018; Radić & Hock, 2011; Zemp et al., 2015), which will have numerous effects on the timing and delivery of nutrients and water to coastal ecosystems (Hood et al., 2009, 2015; Huss et al., 2017; Jenckes et al., 2022, 2023; Milner et al., 2017).

In addition to hydrologic impacts, mountain glaciers increase physical erosion and their advance and retreat reset and alter landscapes (Benn & Evans, 2010; Herman & Braun, 2008). Mountain glaciers increase physical erosion by both mechanical grinding of rocks and increased runoff that elevates the potential for streams to transport sediment (Benn & Evans, 2010). Seasonal advance and retreat of ice in glacierized catchment supplies fresh ground material, and the ongoing long-term trend of retreat due to anthropogenic warming has led to ecological succession and the development of soils (Klaar et al., 2015; Wojcik et al., 2021). Glacier impacts are thus felt throughout

MUÑOZ ET AL. 2 of 24

the watershed. Stream reaches near the glacier record the early succession following glacial retreat and reaches downstream receive fine sediment from upstream and record signals from the later stages of ecological succession (Klaar et al., 2015; Wojcik et al., 2021). This landscape gradient results in varied contributions from different weathering reactions along the watershed. Through its impact on catchment hydrology and landscape evolution, glacierization should modulate the balance of CO_2 -producing and sequestering weathering reactions and thus have direct impacts on the carbon cycle (e.g., Torres et al., 2017).

For these reasons, there has been interest in identifying the influence of glaciers on catchment scale weathering as they modify both the hydrology and landscape characteristics of catchments. Increased physical erosion can increase silicate weathering rates (Riebe et al., 2004) until a tipping point when kinetic and hydrologic controls become important (Maher & Chamberlain, 2014; West, 2012; West et al., 2005). Additionally, erosion drives increased pyrite oxidation, and multiple studies have found that carbonate dissolution dominates instream weathering products even in catchments with only trace amounts of carbonate present (Anderson et al., 2000; Chamberlain et al., 2005; Jacobson et al., 2002; Moore et al., 2013; Torres et al., 2017). This was recently found in a compilation of global glacierized rivers, and led to the hypothesis that the net effect of glacierization may be an additional negative feedback mechanism where carbonate dissolution paired with sulfide oxidation releases CO₂ in excess of silicate weathering, helping prevent runaway glaciation (Torres et al., 2017). Glacierization impacts the hydrology, erosion, and physical characteristics of catchments, all of which can impact the weathering balance of catchments and Earth's climate.

To understand the full impact of glaciers on weathering, their hydrologic impacts must be paired with geochemical tracers of weathering reactions. The behavior of solutes in rivers is often investigated through a concentration-runoff framework (*C-q*), which pairs measurements of solute concentrations and runoff to understand how hydrologic variability impacts solute yields from a catchment. The general form is presented below in Equation 6 (Godsey et al., 2009; Hall, 1970; Moon et al., 2014),

$$C = aq^b (6)$$

where C is concentration (mass solute/volume water), q is runoff (area normalized discharge, in length/time) and a and b are fitting parameters. The fitting parameter b is utilized to describe the behavior of solutes, where a value of -1 is pure dilution (mass of solutes remains the same while volume of water increases), a value of 0 is chemostasis (concentration remains the same regardless of discharge) and a value > 0 indicates increased concentration of solutes with higher discharge (Godsey et al., 2009 see also Bouchez et al., 2017; Ibarra et al., 2017; Torres et al., 2015; Wymore et al., 2017, 2023). The relationships highlighted by the b variable reflect the landscape and hydrologic drivers of solute generation and can be utilized to infer chemical constraints on rock weathering (Clow & Mast, 2010; Ibarra et al., 2017; Torres et al., 2015; Von Blanckenburg et al., 2015). Specifically, once mixing has been accounted for (e.g., rainwater inputs see Tipper et al., 2006) a negative b value indicating solute dilution suggests that catchments are kinetically limited and the speed of dissolution reactions are resulting in decreased concentrations with higher runoff. Since the kinetics of reactions are heavily influenced by temperature, catchments in this weathering regime are strongly influenced by temperature changes as well as modifications to the structure of the critical zone that either change fluid residence times and/or reactive surface area (Gabet & Mudd, 2009; Maher, 2011; West, 2012; West et al., 2005). In contrast, catchments with b values close to 0 (or "chemostatic" behavior) show no change in concentration with a change in runoff. This indicates that fluid and minerals have reached equilibrium (e.g., Winnick & Maher, 2018) and that the availability of fresh minerals as well as thermodynamic constraints on dissolution reactions (e.g., pCO₂) have instead become the limiting factors on solute generation. Variability in C-q relationships provide important insight into the solute-generating processes in watersheds and reflects the dominant weathering regime within watersheds (e.g., Clow & Mast, 2010; Ibarra et al., 2017; Torres et al., 2015; von Blanckenburg et al., 2015), which in turn helps identify sensitivity to driving factors such as climate and tectonics (e.g., Bluth & Kump, 1994; Ibarra et al., 2016; Jenckes et al., 2022; Kump et al., 2000; Maher & Chamberlain, 2014).

To investigate the impact of glacierization on silicate weathering, five catchments with varying glacier cover draining into Kachemak Bay on the southwest side of the Kenai Peninsula were chosen (Figure 1). The largely pristine watersheds lie within the Kachemak Bay State Wilderness Park and National Estuarine Research Reserve, with primary land classes being glacier cover, rocks and exposed sediment, and forest (Table 1). The five catchments were chosen due to their similar climate and underlying geology, and relative ease of access to

MUÑOZ ET AL. 3 of 24

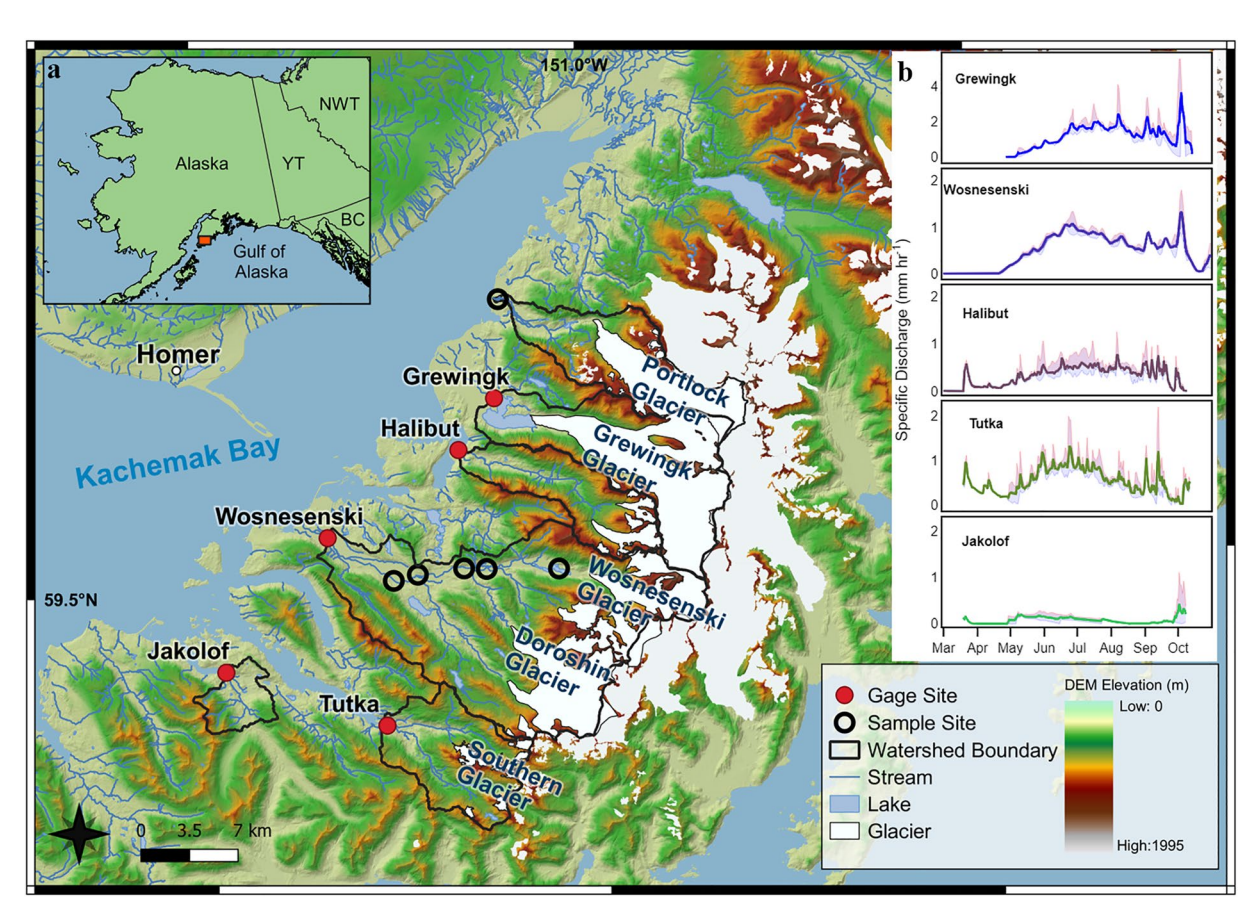


Figure 1. (a) Overview of the study site located in South Central Alaska on the southwest side of the Kenai Peninsula. Red dots show the stream gage locations, and black lines delineate the watersheds. Each catchment is labeled with the watershed name. Open symbols represent the longitudinal sampling in the Wosnesenski and the location of the ungauged sampling site. (b) Average hydrographs from stream-level rating curves in order of glacier cover from high to low for the 5 gauged catchments for 3 years of hydrological data (2019, 2020, and 2021). Red shaded and blue shaded areas represent the minimum, and maximum for the 3 years of data.

facilitate monthly sampling across the seasonal cycle. The hydrographs for all catchments are shown in panel *b* of Figure 1. The more glacierized watersheds have a higher peak in the mid to late summer, whereas the less glacierized watersheds show more influence from rain events (Jenckes et al., 2023). The underlying bedrock geology consists of the McHugh and Uyak complexes. According to Clark (1973), the McHugh Complex is dominated by a metaclastic sequence composed predominantly of gray, gray-green, and dark-green weakly metamorphosed siltstone, graywacke, arkose, and conglomeratic sandstone. It also contains a metavolcanic sequence with greenstones composed of basaltic protoliths and textures that are commonly associated with radiolarian metachert, cherty argillite, and argillite. Additionally, there are small discontinuous outcrops of ultramafic rocks and marble (Clark, 1973). The Uyak complex of Connelly (1978) is similar in character but consists of deformed gray chert and argillite. All of our catchments are experiencing glacier loss (Beamer et al., 2017). Differences in glacier cover with similarities in climate and lithology allow us to utilize a space-for-time substitution framework, with the most glacierized catchment representing one endmember, and the deglacierized catchment representing the final endmember. This framework allows us to examine the influence of variable hydrologic and geomorphic factors associated with glacierization that influence weathering reactions and solute generation in watersheds, and their ultimate impact on the global carbon cycle.

We quantify and partitions solute fluxes between multiple weathering reactions in a series of catchments with varying glacier coverage to understand the effects glacierization and associated landscape changes have on the carbon cycle. To understand how glacierization alters the weathering regime of catchments, we first investigated how discharge conditions impacted solute concentrations over a multi-year seasonal sampling campaign. We then link these observations with an inverse model that partitions solutes to separate weathering reactions to infer the impact of glacierization on the net weathering CO₂ balance in catchments. These inquiries are important for

MUÑOZ ET AL. 4 of 24

Table 1Landscape Characteristics for Study Sites Utilized in MLR

Site id	Description	Watershed area (Km ²)	Avg slope (%)	Glacier cover	Barren cover	Forest cover	Shrub cover	McHugh and Uyak complex	Quaternary alluvium	Jurassic ultramafic	Chugach granitic intrusions
kbtus	Tutka Bay Stream	63.63	22.55	19.1%	37.2%	17.1%	28.4%	79.0%	1.6%	0.3%	0.0%
kbjks	Jakolof Stream	15.77	17.45	0.0%	3.3%	63.8%	30.4%	88.1%	11.9%	0.0%	0.0%
kbhbs	Halibut Stream	55.23	23.65	22.7%	22.7%	6.3%	44.4%	76.3%	0.8%	0.3%	0.0%
kbgws	Grewingk Stream	120.77	13.34	61.0%	13.2%	2.6%	18.9%	35.1%	0.5%	0.6%	0.0%
kbwozs	Wosnesenski Stream	248.60	17.78	36.3%	21.7%	16.5%	25.4%	54.3%	8.6%	0.0%	0.0%
kbpls	Portlock Stream	31.39	20.31	20.5%	21.1%	11.0%	43.2%	71.2%	7.5%	0.0%	0.8%
kbwozlake	Wos lake	44.34	17.60	71.0%	19.7%	0.2%	10.9%	28.9%	0.2%	0.0%	0.0%
kbwozt01	Wos Trib 1	86.75	19.89	46.5%	24.1%	5.0%	24.7%	50.0%	3.1%	0.0%	0.0%
kbwozt02	Wos Trib 2	39.12	13.40	66.0%	17.8%	8.2%	13.1%	33.2%	0.8%	0.0%	0.0%
kbwozt03	Wos Trib 3	71.53	16.14	33.7%	24.4%	20.5%	23.2%	58.4%	5.8%	0.1%	0.0%
kbwozl01	Wos Long 1	87.68	19.89	46.0%	24.0%	5.3%	25.0%	50.1%	3.5%	0.0%	0.0%
kbwozl02	Wos Long 2	130.54	17.88	50.6%	21.7%	6.6%	22.4%	45.6%	3.4%	0.0%	0.0%
kbwozl03	Wos Long 3	212.18	17.20	42.5%	22.2%	13.5%	22.9%	51.1%	5.5%	0.0%	0.0%
kbwozl04	Wos Long 4	215.70	17.17	41.8%	22.0%	14.1%	22.9%	51.1%	6.2%	0.0%	0.0%
kbwozl05	Wos Long 5	248.53	17.79	36.3%	21.7%	16.5%	25.4%	54.3%	8.6%	0.0%	0.0%

constraining controls on the habitability of Earth and other planets over geologic time (Kasting & Catling, 2003; Loper, 2009; Nicholson, 2019) as well as the recovery timescale (e.g., Archer, 2005; Hönisch et al., 2012) of the Earth system due to anthropogenic CO_2 emissions and climate change.

For a more regional view of weathering reactions in high latitude catchments, we refer readers to the companion manuscript by Jenckes et al. (2024). In this contribution, we quantify the effect glacierization has on rock weathering, and then estimate the inorganic weathering CO_2 balance in our catchments. Although the described sites are included in the companion manuscript, we add additional measurements of 87 Sr/ 86 Sr and explore the implications of these added isotopic constraints in estimating weathering reactions. Additionally, here we delve into deeper details of the data and investigate how hydrologic conditions impact the importance of different weathering reactions in catchments through C-q analysis.

2. Methods

2.1. Field Measurements

2.1.1. Water Sampling

The seasonal cycles of solute chemistry and discharge and their data sets were published by Jenckes et al. (2023). Monthly water sampling in the five watersheds spanned March through September of 2019, 2020, and 2021. Jenckes et al. (2023) details the collection methods but we briefly repeat them here. Water samples were collected in 1-L high density polyethylene (HDPE) bottles that were rinsed 3 times with the sample prior to collection. Samples for major elemental analysis were filtered with 0.45 μ m PTFE membrane filters. All samples were kept refrigerated until analysis.

In addition to stream samples, precipitation samples were collected. Precipitation samples were collected in Palmex RS1 Rain Samplers installed in Grewingk and Wosnesenski watersheds near the main gage sites with another RS1 installed at sea level near the Jakolof watershed. To expand our precipitation record, we also consider monthly samples from 2009 to 2021 of precipitation from the nearest National Atmospheric Deposition Program (NADP) precipitation site AK97 (NADP, 2022). In addition to water sampling, stage discharge relationships have been developed for the five primary watersheds (Jenckes et al., 2023).

Stage discharge rating curves were developed at each site using monthly discharge measurements combined with continuous pressure transducer measurements set to 15 min intervals (for more detail see Jenckes et al., 2023). The

MUÑOZ ET AL. 5 of 24

method for discharge measurement varied depending on the discharge conditions. For lower, wadeable discharge conditions, a Marsh McBirney Flo-Mate 2000 or an Ott MF-Pro was utilized. At higher discharges and for all of the Grewingk measurements, a SonTek M9 or S5 Acoustic Doppler Current Profiler (ADCP) was employed. Discharge for all 3 years at the Wosnesenski River was derived from modeled data originating from the work of Beamer et al. (2016) because this stream is highly braided and meandering, thus making manual measurements of a single channel insufficient to categorize total flow. In addition, due to high flow events causing lost equipment at Halibut and Tutka, we used the modeled data for 2021 and 2020 discharges, respectively. Rating curves and discharge measurements were limited to the five primary watersheds, but additional longitudinal sampling along the river corridor was performed to interrogate landscape contributions to weathering fluxes.

2.1.2. Longitudinal Sampling

On two separate occasions (June and September 2021) longitudinal sampling campaigns were taken from the headwaters to the outlet of the Wosnesenski catchment (see Figure 1). The mainstem was sampled at regular intervals and each major tributary was also sampled (Figure 1). In comparison to the regular seasonal sampling at the outlet, these snapshot campaigns allowed for a longitudinal synoptic view of the watershed. Sampling protocols described above for the main outlet sites were followed. In addition to water samples, representative rock samples were collected to constrain the silicate weathering endmember.

2.1.3. Rock Samples

Large river cobbles were taken from each of the 5 catchments. The focus was on the selection of large hand samples that were not strongly weathered and representative of the bedrock lithology.

2.2. Analysis

2.2.1. Aqueous Chemistry: Major Anions and Cations

Water samples were analyzed for major ($[Ca^{2+}]$, $[Mg^{2+}]$, $[Na^{+}]$, $[Cl^{-}]$, $[SO_4^{2-}]$), and trace element ($[Sr^{2+}]$) concentrations at SGS Environmental Services in Lakefield, Ontario. Inductively coupled plasma mass spectrometry (ICP-MS) was used for elemental analysis using the methods SM 3030/EPA 200.8. Anions were analyzed by ion chromatography following the methods in EPA300/MA300-inos1.3. All elemental analytical error was reported to be less than 10% (Jenckes et al., 2023).

2.2.2. 87Sr/86Sr Isotope Analysis

Filtered water samples (0.45 μ m) were purified using ion exchange chromatography in the PicoTrace clean lab at Brown University. Sufficient water to contain 200 ng of Sr was evaporated (1–7 ml) to dryness in an acid-cleaned Savillex beaker, and then reconstituted in 1,000 μ l of 3 N ultrapure HNO₃ before chromatographic processing with Sr-spec resin (Eichrom) filled micro-columns. Collections from the columns were analyzed for ⁸⁷Sr/⁸⁶Sr isotopes at the Mass Spectrometer Analytical Facility at Brown University using a Thermo Scientific NEPTUNE PLUS multicollector ICP-MS (Mallick et al., 2023). Sr was introduced into the plasma using a PFA nebulizer at a rate of ~100 μ l min-1 coupled with an APEX-IR introduction system. We utilized H sampler and H skimmer cones. ⁸⁷Sr/⁸⁶Sr was corrected for instrumental mass fractionation using ⁸⁸Sr/⁸⁶Sr = 0.1194 following an exponential law. Sr isotope ratios for the samples are reported relative to the ⁸⁷Sr/⁸⁶Sr of NBS SRM 987 (0.71024) and were measured at 100 ppb concentration. Long-term reproducibility of ⁸⁷Sr/⁸⁶Sr of NBS SRM 987 was 21 ppm over the course of the measurements ($2\sigma n = 31$).

2.2.3. Whole Rock Analysis

Rocks were powdered with a ball mill and analyzed utilizing LiBO₂ Fusion and ICP AES and ICP-MS at SGS Environmental Services in Lakefield Ontario with methods GO_ICP95A50, and GE_IMS95A50. All elements utilized in the analysis were within the upper and lower bounds of detection for all of the samples.

2.2.4. Water Sample Quality Assurance (QA)

We only considered samples suitable for analysis that met quality criteria (QC) following Cole et al. (2022), where samples with a milli-equivalent sum of anions ([Cl $^-$], [SO $_4^2$ $^-$]) greater than the milli-equivalent sum of cations ([Ca 2 +], [Mg 2 +], [Na $^+$]) were rejected. All of our river chemistry samples met this criterion. For the NADP precipitation samples station (AK97) we expanded this and utilized all reported chemistry, which included

MUÑOZ ET AL. 6 of 24

 Table 2

 Endmember Compositions Used in Inverse Geochemical Mixing Model (MEANDIR)

		Precipitation	Silicate	Carbonate	Pyrite	Clay
$[Na^+]/\Sigma^{\pm}$	Min	0.24	0.012	0	0	0
$[Na^+]/\Sigma^\pm$	Max	0.88	0.57	0	0	0.5
$[Ca^{2+}]/\Sigma^{\pm}$	Min	0	0.038	0.5	0	0
$[Ca^{2+}]/\Sigma^{\pm}$	Max	0.47	0.54	1	0	0.5
$[Mg^{2+}]/\Sigma^{\pm}$	Min	0	0.17	0	0	0
$[Mg^{2+}]/\Sigma^{\pm}$	Max	0.19	0.75	0.5	0	0.65
$[Cl^-]/\Sigma^\pm$	Min	0.24	0	0	0	0
$[Cl^-]/\Sigma^\pm$	Max	1	0	0	0	0
$[\mathrm{SO_4}^{2-}]/\Sigma^{\pm}$	Min	0	0	0	1	0
$[\mathrm{SO_4}^{2-}]/\Sigma^{\pm}$	Max	0.52	0	0	1	0
$[Sr^{2+}]/\Sigma^{\pm}$	Min	0	9.58E-04	5.00E-04	0	0.00001
$[Sr^{2+}]/\Sigma^{\pm}$	Max	3.26E-03	2.51E-03	4.00E-03	0	0.003
⁸⁷ Sr/ ⁸⁶ Sr	Min	0.7091	0.704	0.7068	0	source
⁸⁷ Sr/ ⁸⁶ Sr	Max	0.7093	0.706	0.7081	0	source

Gray cells are only applicable and used in inversion scenario 2 which includes 87Sr/86Sr isotope measurements.

the cations and anions above as well as $[K^+]$, $[NH_4^+]$, and $[NO_3^{3-}]$. Of the 89 NADP samples, 7 met this criterion, while out of our 10 collected precipitation measurements, 6 met this criterion.

2.3. Geochemical Mixing Model

A Monte Carlo inversion model (MEANDIR) developed and described by Kemeny and Torres (2021) predicts the contribution of solute sources to stream chemistry, given a prescribed set of endmember chemical compositions. For our inversions, the endmembers utilized in the inversion are silicate, carbonate, clay, precipitation, and pyrite. Their ranges are shown in Table 2. All the endmembers serve as solute sources except for clay, which serves as a solute sink. The model utilizes observed river chemistry and user defined endmember chemical and isotopic compositions as inputs and generates fractional contributions from each endmember (F_{endmember}) as outputs. Analogous methods have been widely utilized to constrain the silicate weathering from river chemistry (Burke et al., 2018; Cole et al., 2022; Gaillardet et al., 1999; Hemingway et al., 2020; Kemeny & Torres, 2021; Moon et al., 2014; Négrel et al., 1993). Here we utilize the notation and conventions presented in Kemeny and Torres (2021) to visualize and invert our samples.

For visualization and comparison between samples and the inferred endmembers, each element is normalized by the μM sum of the cations in each sample or endmember where

$$\Sigma^{+} = \left[\text{Ca}^{2+} \right] + \left[\text{Mg}^{2+} \right] + \left[\text{Na}^{+} \right] \tag{7}$$

With this convention, each element in the normalization cannot have a value greater than one, and thus $[Ca^{2+}]/\Sigma^+ + [Mg^{2+}]/\Sigma^+ + [Na^+]/\Sigma^+$ is equal to 1. An elemental ratio $([X]/\Sigma^+)$ for example, can be thought of as the proportion of X out of all the weathering cations.

In the inversion, pyrite oxidation contributes to solutes ($[SO_4^{2-}]$) and is therefore included in the normalization as shown below in Equation 8.

$$\Sigma^{\pm} = \left[\text{Ca}^{2+} \right] + \left[\text{Mg}^{2+} \right] + \left[\text{Na}^{+} \right] + \left[\text{SO}_{4}^{2-} \right]$$
 (8)

This normalization differs from previous commonly utilized single solute normalizations (Gaillardet et al., 1999), but has the advantage of including all solute generating weathering reactions, as presented in detail in Kemeny and Torres (2021). Each inversion iteration generates the $[X]/\Sigma^{\pm}$ (where [X] is the solute of interest $[Ca^{2+}]$,

MUÑOZ ET AL. 7 of 24

[Mg²⁺], [Na⁺], [Cl⁻], [SO₄²⁻]) for each element in each endmember by pulling a value randomly from the uniform distribution presented in Table 2, and the criteria for a successful iteration is that the river sample is reconstructed by the end member contributions following the mass balance equations (Equations 9 and 10) below, allowing for a 15% misfit from the river sample.

$$[X]/\Sigma^{\pm}_{\text{river}} = ([X]/\Sigma^{\pm})_{\text{precip}} \times F_{\text{precip}} + ([X]/\Sigma^{\pm})_{\text{silicate}} \times F_{\text{silicate}} + ([X]/\Sigma^{\pm})_{\text{carbonate}} \times F_{\text{carbonate}} + ([X]/\Sigma^{\pm}_{\text{pyrite}}) \times F_{\text{pyrite}} - ([X]/\Sigma^{\pm}_{\text{clay}}) \times F_{\text{clay}}$$

$$(9)$$

$$F_{\text{precip}} + F_{\text{silicate}} + F_{\text{carbonate}} + F_{\text{pyrite}} - F_{\text{clay}} = 1$$
 (10)

Where F_{precip} , F_{silicate} , $F_{\text{carbonate}}$, F_{pyrite} , F_{clay} are the fractional contribution or proportion of dissolved ions from each endmember to the ion concentrations [X] in the river sample. A similar form of this equation can be utilized to include isotope ratios, and is included in Supporting Information S1 (Equation S1). Each sample is inverted 100,000 times and the 200 samples which best reconstruct the observed river chemistry with a mass balance of $\pm 15\%$ of the original sample are retained (See Kemeny & Torres, 2021). We utilize the median of retained simulation results for our calculations and take the 25th and 75th percentiles as the inversion error.

2.3.1. Endmember Assumptions

The endmember uniform distributions utilized in the inversion are summarized in Table 2. Our silicate and precipitation end members are based on the range observed in our sample set. We utilized the 5 representative rock samples to constrain the range of our inversion's silicate end members. Due to the limitations of a small sample size, we expand the range by ± 0.2 (i.e., 20%) in the normalization. For the precipitation end member, we take a similar approach. After we screened the precipitation data (NADP and our own stations) for quality assurance and control, we took the minimum and maximum values observed and increased the bounds by 10%. By utilizing observations from gauges to define our precipitation endmember instead of assuming seawater like composition, our precipitation endmember encapsulates variations that may arise from forms of atmospheric deposition other than seaspray. Although we do not expect a high SO₄ contribution from atmospheric deposition in this region (Gao et al., 2018), others working nearby have observed anthropogenic contributions to SO₄ deposition on glaciers (Nagorski et al., 2019). We note that the observations used to define the precipitation endmember demonstrate higher $[SO_4^{2-}]/[Na^+]$ ratios (mean 0.366 ± 0.288) than average seawater (0.06, seawater compositions taken from Morcos, 1970). The carbonate endmember is defined by allowing up to 50% substitution with Mg (e.g., Torres et al., 2016). We chose not to incorporate an evaporite endmember for sulfate contributions following Kemeny et al. (2021) because evaporite minerals have not been directly observed or described in the geologic units of the Mchugh and Uyak complexes, or any of the other minor geologic units observed in our watersheds (Clark, 1973; Connelly, 1978). Additionally, our rivers have low [Cl-] concentrations (median 39.50 µMol/l, 25th percentile 28.21 µMol/l, 75th percentile 56.41 µMol/l) and over half (62%) of our data points have $[SO_4^{2-}]/[Cl^-]$ ratios greater than the $[SO_4^{2-}]/[Cl^-]$ ratio for evaporites given in Burke et al. (2018)—defined based on the mineral abundances in evaporites given in Lerman et al. (2007)—indicating that the source of SO₄²⁻ cannot contribute significant Cl⁻ to make up the composition of our samples. Due to the marine metasedimentary lithology of our catchments, we define this endmember as Pyrite, which serves as a pure source of SO₄²⁻. The clay endmember functions as a sink, removing cations (Ca²⁺, Mg²⁺, Na⁺, Sr²⁺) from the solution and can explain the observation of river chemistry that cannot be described by conservative mixing of the other endmembers alone (Kemeny & Torres, 2021). Due to the lack of suitable measurements of secondary phases, we set a wide range for possible clay end member compositions, which allows the inversion to define and utilize the composition of clay endmember that is necessary to produce the observed river data (Kemeny & Torres, 2021). A similar approach has been utilized by Cole et al. (2022), who faced similar difficulties in characterizing secondary phyllosilicate minerals due to glacial grinding producing fine grained material of mixed primary and secondary mineral origin.

For the inversions that include 87 Sr/ 86 Sr isotopes, the values of [Sr $^{2+}$] concentration and the 87 Sr/ 86 Sr composition of the endmembers were selected based on geologic history (i.e., depositional age and associated seawater 87 Sr/ 86 Sr) and are listed in Table 2. For the precipitation endmember, we utilize [Sr $^{2+}$] concentrations of modern seawater (Lebrato et al., 2020) and 87 Sr/ 86 Sr isotope ratios of modern seawater (Chen et al., 2018) following previous authors (Cole et al., 2022; Schopka et al., 2011). For the silicate [Sr] concentrations, we follow the same assumptions for the major elements and utilize $\pm 20\%$ the observed range of [Sr] concentrations of rock samples. Since the McHugh and Uyak complexes consist of partially metamorphosed oceanic sediments that

MUÑOZ ET AL. 8 of 24

have interacted with mantle fluids, we utilize mantle like values taken from Geilert et al. (2020) for the ⁸⁷Sr/⁸⁶Sr ratio of silicates. For the carbonate [Sr] concentrations, we utilize the range of ocean values at the time of lithification of the metasedimentary rocks taken from Lebrato et al. (2020), and similarly constrain the isotopic values with the seawater range of ⁸⁷Sr/⁸⁶Sr spanning the age range of the lithified sediments (Chen et al., 2018).

2.3.2. Inversion Scenarios

Our first inversion scenario (Major ion inversion) utilizes major anion ([Cl $^-$], [SO $_4^{2-}$]) and cation ([Na $^+$], [Mg $^{2+}$], [Ca $^{2+}$]) concentrations as inputs with precipitation, silicates, carbonates, pyrite, and clay as possible endmembers. We select these major ions due to their largely conservative behavior in transport, which allows us to calculate the overall impact of weathering reactions on the carbon cycle (Kemeny et al., 2021). We note that while [Na $^+$] often undergoes ion exchange, we see negligible evidence for this in our stream water chemistry detailed in Supporting Information S1 (Figure S3). We avoid using [K $^+$] and dissolved [SiO $_2$] because although they are sourced from weathering reactions, they are biologically cycled and their concentration in rivers has been shown to reflect this (Chaudhuri et al., 2007; Derry et al., 2005). Additionally, we do not focus on [HCO $_3$ $^-$] since it is not conservative due to riverine exchange with the atmosphere (Raymond et al., 2013) and riverine metabolism (Quay et al., 1995). The second inversion scenario (Isotopic inversion) retains the same endmembers and elemental bounds but includes 87 Sr/ 86 Sr as an additional input and constraint. For both inversions, we run a maximum of 100,000 iterations to achieve 200 successful inversions, which are defined as samples where the mass balance of reconstructed samples is within 15% of the observed stream chemistry.

2.4. C-q Analysis

2.4.1. Solute C-q Power Law Fits

Utilizing our continuous record of discharge paired with point measurements of concentration, we fit power law Equation 6 for each of our 5 catchments to relate the concentration of major solutes to runoff (e.g., Godsey et al., 2009; Ibarra et al., 2017; Moon et al., 2014). We do not have enough data to robustly develop C-q relationships for all samples with Sr isotopic data, so C-q analysis is carried out on the major ion inversion results only.

2.4.2. Fraction *F-q* Power Law Fits

Similarly, we utilize the major ion inversion model output contribution from each end member with paired runoff measurements to fit power law Equation 11, expanding upon the approach from Moon et al. (2014), and Ibarra et al. (2017), who utilized this form to fit the contribution from precipitation at various discharges.

$$F_{\text{endmember}} = aq^b \tag{11}$$

Where $F_{\rm endmember}$ is the modeled output fractional contribution (sink in the case of clay) to total solutes from each endmember (Silicate, Carbonate, Precipitation, Pyrite, Clay), q is runoff in mm/d and a and b are the same fitting parameters discussed in Equation 6 in the introduction. Similar to the C-q analysis, we do not have enough data to develop F-q relationships for the isotopic inversion and limit our F-q analysis to the major ion inversion. Utilizing the fitted relationships Equations 6 and 11 produce modeled concentration and $F_{\rm endmember}$ contributions with discharge as input. These modeled $F_{\rm endmember}$ contributions and concentrations were utilized in our estimates of weathering fluxes described below.

2.5. Area-Normalized Flux Estimates

To incorporate the inversion error in our flux estimates, we calculated an inverse variance weighted average at each site for each $F_{\rm endmember}$ for both inversion scenarios. We use this average $F_{\rm endmember}$ and its variance to propagate the inversion uncertainty through our flux calculations. We acknowledge that there are further uncertainties including discharge estimation and analytical uncertainty of the major ions and note that the treatment of error in this way assumes that inversion is the largest source of uncertainty in our flux estimate.

2.5.1. Flux Estimates With Averaged Values

We estimate solute fluxes utilizing average concentration and average discharge for both the major ion and isotopic inversion for each catchment following the literature (Bluth & Kump, 1994; Gaillardet et al., 1999; Gislason et al., 1996; Torres et al., 2017). This approach assumes that catchments are largely chemostatic, and

MUÑOZ ET AL. 9 of 24

concentrations of solutes do not change with discharge. We calculate total cation yield using average concentration and average discharge, and partition weathering contributions from each endmember using an inverse variance weighted average $F_{\text{endmember}}$ for each catchment for each inversion scenario.

As our discharge records do not span the entire year, we report our flux estimates in two different forms. When comparing between our catchments with varying discharge record lengths (115–200 days), we normalize to the length of the discharge record, which gives a daily flux estimate. When compared to literature values of yearly solute fluxes, we utilize this average daily value and multiply it by the average number of days in the 3 years of discharge records. This means that our yearly flux estimates are conservative and are therefore minimum flux estimates, as they assume that there is no solute flux during the times not captured by the discharge record. Considering that these streams freeze over and see reduced flow in the wintertime, we consider our estimates to represent the majority of solute fluxes (Beamer et al., 2017).

2.5.2. Flux Calculations With *C-q* Relationships

To investigate the impact of hydrologic conditions on flux estimates, we also estimated fluxes using fitted parameters and our continuous discharge measurements for the major ion inversion, which had suitable data density for this method. This method allows us to model continuous concentration and $F_{\rm endmember}$ contributions, as described in the preceding sections. Here, the flux is calculated for each catchment utilizing Equation 12 below.

$$Flux = F_{\text{endmember}}^* \times C^* \times q \tag{12}$$

Where $F_{\rm endmember}^*$ is modeled fractional contribution to total solutes from each of the endmembers calculated utilizing fitted parameters and Equation 11, C^* is modeled concentration for each solute utilizing Equation 6, and q is the continuous runoff record. To propagate the error associated with the inversion, we utilize the variance for each catchment's average $F_{\rm endmember}$ as the variance for $F_{\rm endmember}^*$. Since q is at a daily resolution, this produces a continuous flux estimate for each day captured by the runoff record. Where the calculated b value for either $F_{\rm endmember}^*$ or C^* fits was within one standard error of 0, the average value of $F_{\rm endmember}^*$ or C^* was utilized. Summing the estimates for each day produces a total flux estimate and summing the square of the errors produces a variance associated with this estimate.

2.5.3. Weathering CO₂ Balances

To convert the cation yields to long-term CO_2 consumption fluxes, we use the stoichiometry presented in Equation 1 and Equation 2, and the calculated $[Ca^{2+}]$ and $[Mg^{2+}]$ ions derived from silicate weathering. Additionally, we include 30% of the $[Na^+]$ assuming it will undergo cation exchange over its residence time in the ocean and release additional $[Ca^{2+}]$ and $[Mg^{2+}]$ following Galy et al. (1999). For CO_2 production, we utilize the stoichiometry in Equation 5 and assume all pyrite oxidation occurs in the presence of carbonates, which is supported by our metasedimentary lithology and elevated carbonate fluxes.

2.6. Geospatial Analysis

2.6.1. Catchment Attributes and Land Cover

Geographic analysis was completed using R and open-source packages (R Core Team, 2023). Catchment attributes in Table 1 were calculated using the R packages rgrass7 (Bivand, 2023) and open STARs (Kattwinkel et al., 2020) with the NLCD land cover map 2016 (Dewitz & USGS (US Geological Survey), 2021) and the state geologic map of Alaska (Wilson et al., 2015). We derived stream networks utilizing the 90m resolution Multi-Error-Removed Improved-Terrain Digital Elevation Model (MERIT DEM) (Yamazaki et al., 2017) and the rgrass7 function r.stream network with flow accumulation set to 3000. This value was manually selected through trial and error and visual interpretation to optimize the visual match to the stream network observed in satellite imagery. The NLCD 2016 land cover map (Dewitz & USGS, 2020) has been shown to have an overall accuracy of 86.4% (s.e. 0.6%) (Wickham et al., 2021). The state geologic map of Alaska comes from a compilation of paper geologic maps (Wilson et al., 2015) that were produced at the 1:25,000 scale that is standard for the state of Alaska. The MERIT DEM has a resolution of 90 m and maps 58% of the global land area with ± 2 m or better vertical accuracy (Yamazaki et al., 2017). Our estimates of percent glacier cover differ slightly from Jenckes et al. (2023) because we utilized the glacial cover estimated in the geologic map, while they utilized a more advanced classification system. Their estimates are more accurate representations of glacial cover, but we utilize the values from the geologic map so that they are consistent with the lithologic units in our regression.

MUÑOZ ET AL. 10 of 24

21699011, 2024, 3, Downloaded from https://agupubs.onlinelibrary.wiley.com/doi/10.1029/2023JF007255 by University Of Alaska Fairbanks, Wiley Online Library on [09/10/2024]. See the Terms

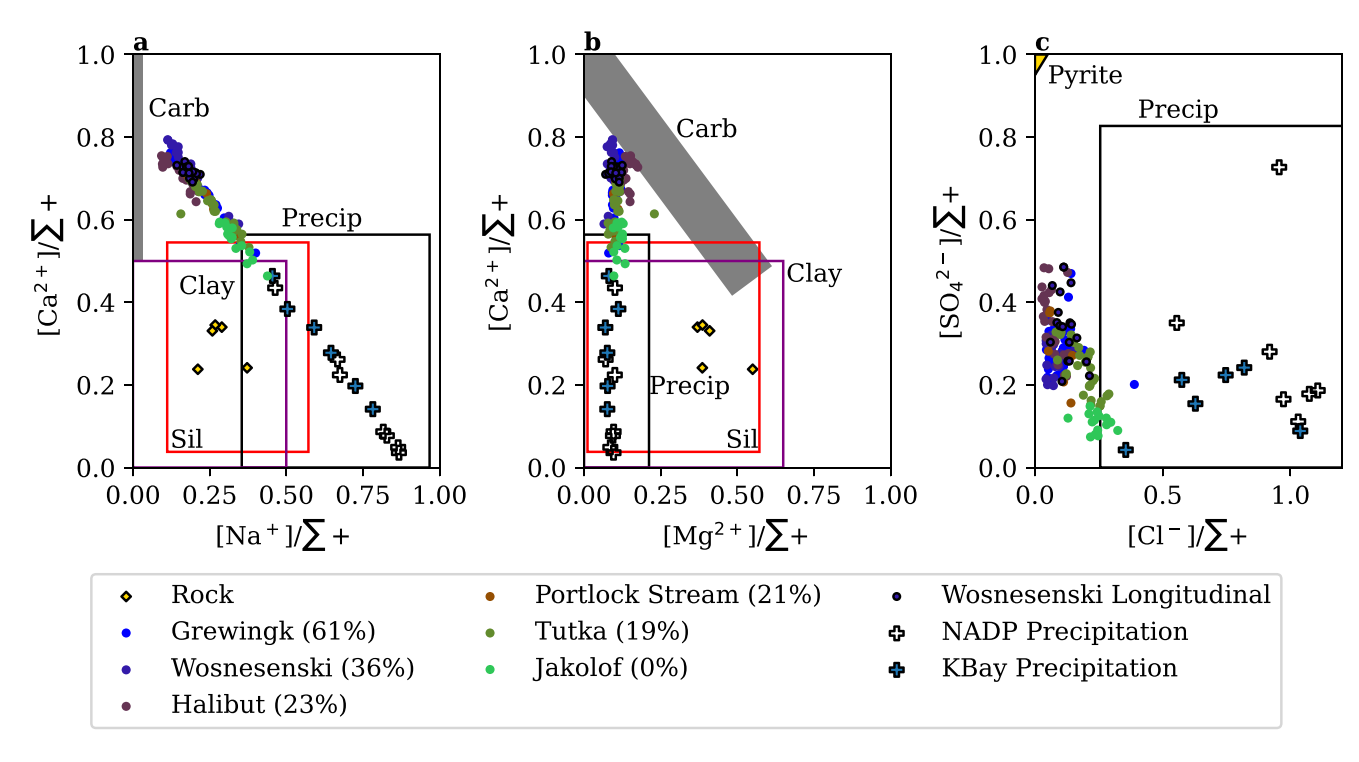


Figure 2. Quality controlled river chemistry for the 5 gauged sites as well as one ungauged site and the longitudinal transect (circles), precipitation (plus), and rock (diamond) data with inferred endmembers in boxes. Watersheds are distinct but see some overlap. (a) $[Na^+]/\Sigma + \text{versus}$. $[Ca^{2+}]/\Sigma + \text{Water}$ samples indicate mixing between precipitation, silicate, and carbonate end members more glacierized watersheds are closer to the carbonate endmember and less glacierized watersheds are closer to precipitation and silicate end members. (b) $[Mg^{2+}]/\Sigma + \text{versus}$. $[Ca^{2+}]/\Sigma + \text{Same}$ mixing trend as in a, but with some evidence for potential mixing with silicate end member (c) $[Cl^-]/\Sigma + \text{versus}$ $[SO_4^{2-}]/\Sigma + \text{Nearly}$ all samples from glacierized catchments have a higher proportion of their solutes attributed to sulfate than from the non-glacierized catchment (Jakolof 0%), and there are non-negligible contributions from precipitation. All points fall between pyrite and precipitation, with some river chemistry points approaching the precipitation endmember.

2.6.2. Multiple Linear Regression (MLR) of Catchment Characteristics and Endmember Contributions

To understand the empirical relationship between catchment properties and weathering reactions, the contributions from each $F_{\rm endmember}$ were predicted by stepwise multiple linear regression using ordinary least squares. These regressions were completed using the python package statsmodels (Seabold & Perktold, 2010). All catchment characteristics (Table 1) were included to create an initial model that was refined by removing the variables with the least explanatory power based on the highest and least significant p values and run iteratively to achieve a model with the lowest Akaike information criterion (AIC). The resulting models are presented in Table S1 in Supporting Information S1.

3. Results

3.1. Stream Chemistry

Measurements of major stream chemistry are displayed as points in the Σ^+ cross plots in Figure 2, with inferred end members displayed as binding boxes. The points from seasonal sampling in each catchment fall along mixing lines between end members, implying changes in the relative contributions from each end member. Chemical signatures of each watershed group separately, and all watersheds generally fall on a mixing line between the precipitation, silicate, and carbonate endmembers. While the distribution in measurements from different catchments overlap, they are generally distinct from one another. The precipitation measurements (both ours and the NADP points) also fall along a mixing line. In most catchments, the river chemistry is strongly influenced by the carbonate end member, and the less glacierized catchments fall furthest from the pyrite end member.

3.2. MEANDIR Outputs

The major ion (inversion scenario 1) and isotopic inversion (inversion scenario 2) show convergent behavior in both predicted endmembers (Figure 3a) and their fractional contributions (Figures 3b and 3c; Figure S5 in

MUÑOZ ET AL. 11 of 24



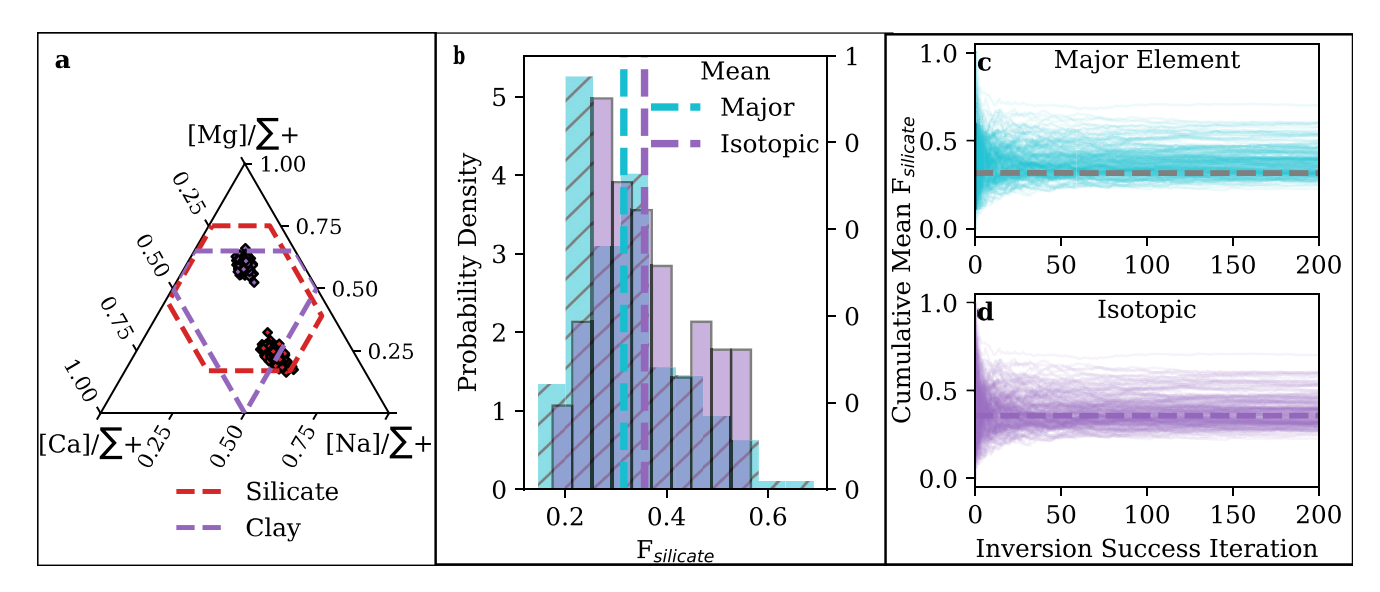


Figure 3. Geochemical inversion outputs. (a) Lithologic endmember results. Dotted lines show inferred endmembers which were the constraints on the inversion, and points show the end member utilized by the inversion for each sample. Carbonate endmembers are not shown as they have no [Na] and all plot between 0.5 and 1 on $[Ca]/\Sigma+$. (b) Density distributions for modeled fraction of solutes from silicate weathering. Dotted lines show the mean for both major ion and isotopic inversions. The isotopic inversion, which includes ${}^{87}Sr/{}^{86}Sr$, increases the predicted contribution from silicate weathering. (c, d). The cumulative mean of one of the modeled parameters (Fraction solutes from silicate weathering) for all samples as a function of inversion success iteration. Success is determined whether the parameters reconstruct the original sample $\pm 15\%$. Both the major ion inversion c and the isotopic inversion d converge after only 50 samples that have met mass balance constraints.

Supporting Information S1). Inversion predicted lithologic endmembers for the major ion inversion are shown in Figure 3a. The clay endmember is predicted to have high [Mg], while the predicted silicate end member has lower [Mg] concentrations than our bulk rock samples. Mean behavior for an example parameter (Fraction of solutes from silicate weathering, $F_{\rm silicate}$) for all samples is shown in Figures 3c and 3d, converging quickly after about 50 samples meet mass balance constraints. The isotopic inversion results in a ~4% increase in the mean $F_{\rm silicate}$ (from 32% to 36%) and a comparable decrease in the mean fraction from carbonate weathering $F_{\rm carbonate}$ (59%–52%). Differences between major ion and isotopic inversion mean $F_{\rm silicate}$ and $F_{\rm carbonate}$ are both significant at p < 0.001 when compared with an inverse variance weighted welches T-test. The change and the distribution of values are shown for the $F_{\rm silicate}$ in Figure 3b, and for all $F_{\rm endmembers}$ in Figure S5 in Supporting Information S1. Endmembers across catchments and the $F_{\rm endmember}$ predicted by the inversion model converge, with the isotopic inversion predicting higher contributions from silicate weathering and lower contributions from carbonate weathering.

3.3. Landscape Analysis

Land cover, geology, slope, and watershed area for the 5 gauged sites as well as an additional routinely sampled site (Portlock Stream) and the eight sites in the longitudinal transect (Wosnesenski) were calculated and are shown in Table 1. The sites range from 0% to 61% glacier cover, with dominant land types being snow and ice, barren, forest (combined deciduous (lu 41) and evergreen (lu 42)) and shrub (combined lu 51 and lu 52). In all watersheds the primary geology is the McHugh and Uyak complexes (33%-88%) with some small outcrops (less than 0.5%) of mafic and ultramafic rocks in 8 catchments and small outcrops of granitic rocks (0.8%) in one catchment (Portlock). Quaternary alluvium makes up from 0.5% to 11% of the watershed. No geologic unit is assigned to regions covered by ice, which explains the remaining deficit in geologic cover. Average slopes in the catchments are comparable and range from 13 to 23°. The best model (lowest AIC) predicting the fraction of solutes from each weathering end member (silicate, carbonate, pyrite and clay) utilizing catchment characteristics, land and geologic cover as predictor variables are shown in Supporting Information S1 (Table S1). Silicate fractions are best predicted by the presence of small outcrops of ultramafic and granitic rocks, as well as increases in forest cover. Carbonate contributions are predicted by increases in the slope, and land cover classes barren, forest, and shrub, and the presence of Jurassic ultramafics. We find decreases in carbonate contributions with increasing cover that is quaternary alluvium and the McHugh and Uyak complex. We find that pyrite contributions are best predicted by lower forest and barren cover as well as reduced ultramafic and granitic bedrock. Our

MUÑOZ ET AL. 12 of 24

21699011, 2024, 3, Downloaded from https://agupubs.onlinelibrary.wiley.com/doi/10.1029/2023JF007255 by University Of Alaska Fairbanks, Wiley Online Library on [09/10/2024]. See the Terms

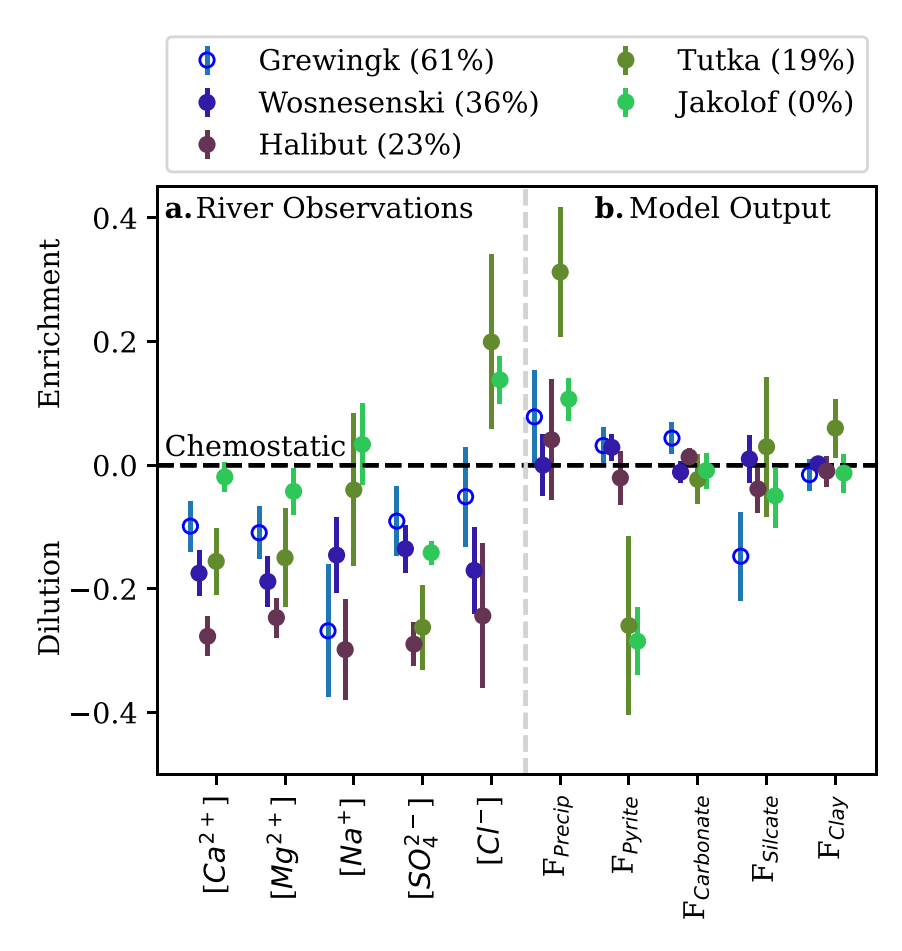


Figure 4. *C-q* Relationships: Fitted b values for river observations and modeled solute contributions from endmembers. Values above the chemostatic line indicate solute enrichment at higher runoff, while those below indicate dilution at higher runoff. We note that the Tutka consistently has the largest error bars stemming from the uncertainty in the geochemical inversion. This could be because the Tutka is made up of two similarly sized tributaries with unequal glacier cover (Figure 1), meaning that the Tutka fluctuates between being dominated by one or the other. (a) We observe significant dilution in glacierized catchments, and less dilution and even some enrichment in less and non-glacierized catchments. The Grewingk watershed is shown in open circles because it has a large proglacial lake that modifies stream chemistry evident in minor dilution behavior. (b) Fraction of solutes from endmembers. The Wosnesenski (36%) and Halibut (23%) are close to chemostatic meaning that contributions from different endmembers do not change with discharge, while the Tutka (19%) and Jakolof (0%) see enrichment from precipitation at higher discharge, and lower contributions from pyrite at higher discharge. Jakolof (0%) sees reduced contributions from the silicate endmember at higher discharges.

regressing performs less well on Clay contributions, which are best predicted by decreased glacier cover, quaternary alluvium, and ultramafic rock. All catchments have similar geology and vary primarily in their glacier, forest and shrub cover, which can be utilized to predict a fractional contribution from different end members.

3.4. Concentration-Runoff Analysis

Analysis of concentration-runoff (C-q) relationships for the major ion inversion shows contrasting responses between glacierized and non-glacierized catchments (Figure 4a). The Grewingk (61% glacial cover) differs in its patterns from other glacierized catchments because its glacial outlet has a large proglacial lake that buffers stream chemistry. We observed moderate to low dilution (b < 0) in all solutes. Wosnesenski (36% glacier cover) and Halibut (23% glacier cover) show dilution in all major solutes, with the Halibut having the greatest dilution overall. The Tutka (19% glacier cover) shows dilution in $[Ca^{2+}]$, $[Mg^{2+}]$, and $[SO_4^{2-}]$, chemostasis (b value = 0) in $[Na^+]$, and enrichment (b value > 0) in $[Cl^-]$. The Jakolof (glacier cover 0%) shows near chemostatic values for $[Ca^{2+}]$, $[Mg^{2+}]$, and $[Na^+]$ with dilution comparable to the more glacierized catchments in $[SO_4^{2-}]$ and enrichment in $[Cl^-]$. Our results indicate that any amount of glacier cover produces stronger dilution patterns, and our non-glacierized catchment has near chemostatic behavior.

MUÑOZ ET AL. 13 of 24



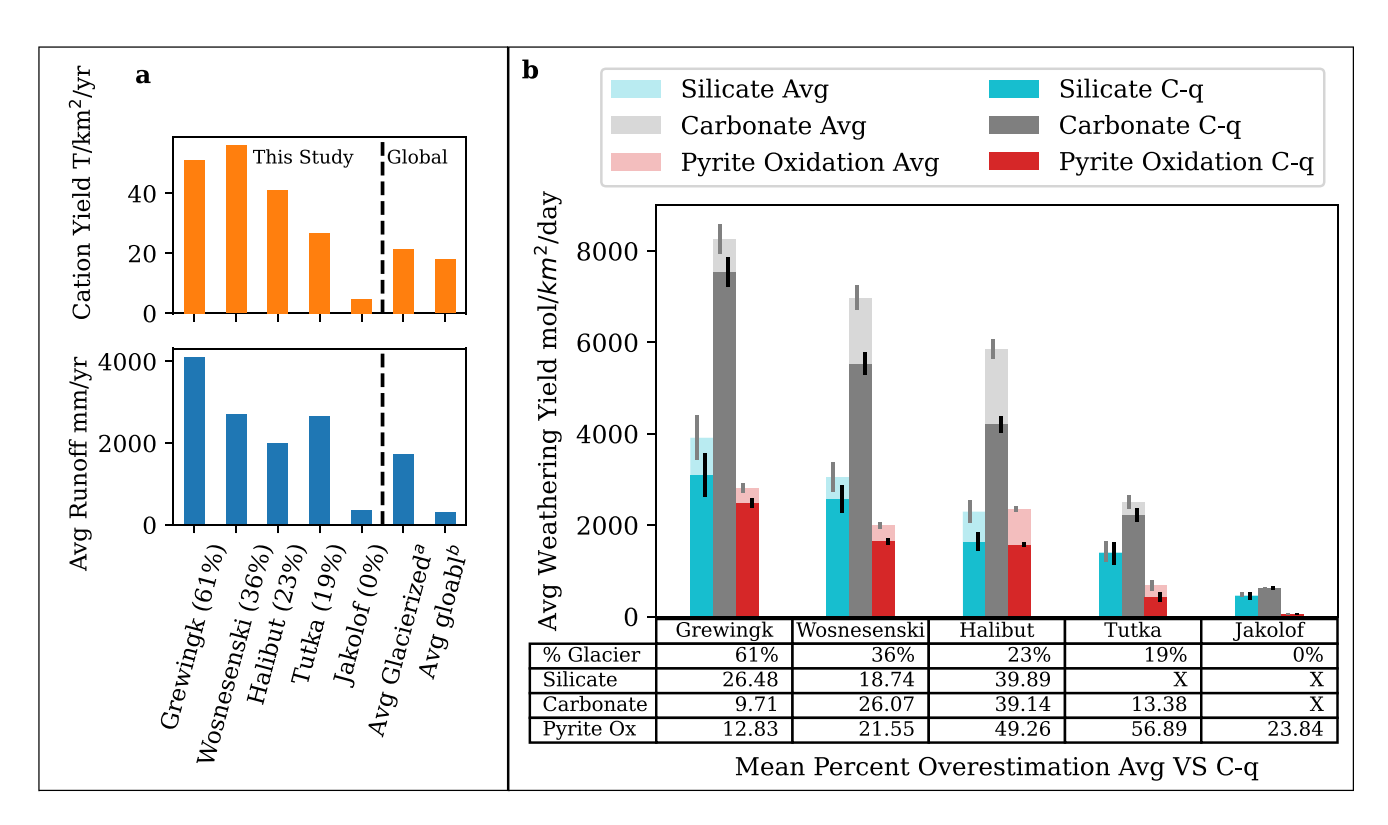


Figure 5. Cation yields, runoff, and solute partitioning. (a) Cation yields and watershed runoff compared to global values. We find that all of our catchments have yields above the compiled glacierized catchment average, except for the non glacierized catchment which has lower yields than the average for global rivers. Runoff follows this same trend. (b) Cation yields partitioned to weathering reactions utilizing average concentration and discharge as well as C-q relationships. Error bars represent $\pm \sigma$. We find that estimates utilizing average concentration and discharge overpredict all weathering fluxes in glacierized catchments, but are suitable for non-glacierized catchments. We find elevated weathering fluxes from all reactions in our glacierized catchments. ^aData from Torres et al. (2017) ^bData appears in Torres et al. (2017) but is from Gaillardet et al. (1999).

Analysis of fraction runoff (F-q) relationships similarly shows variations in response between glacierized and non glacierized catchments (Figure 4b). Grewingk (61%) shows small amounts of enrichment in contributions from precipitation, pyrite oxidation, and carbonate weathering, with some dilution in silicate weathering. Wosnesenski (36%) retained steady fractional contributions from each endmember across runoff conditions, indicating constant proportional contributions to the solute load from each endmember regardless of flow. Halibut (23%) follows a similar pattern, with some slight increase in the contribution from precipitation at higher runoff, and diminished contributions from pyrite oxidation. The Tutka (19%) demonstrates the highest enrichment from precipitation and the greatest dilution in pyrite contributions, with near chemostatic values for carbonate, silicate, and clay. Jakolof (0%) shows similar increased contributions from precipitation and decreased contributions from pyrite, with steady contributions from carbonates and some dilution in both silicate and clay endmembers. With increasing runoff, the more glacierized catchments see little or no change in the fractional contributions from pyrite oxidation, and the non-glacierized catchments see lower contributions from silicate and clay endmembers. The Grewingk watershed departs from the other watershed trends likely due to its proglacial lake.

3.5. Flux Calculations

3.5.1. Cation Yields and Weathering Cation Fluxes

Total cation yields and weathering related cation fluxes are larger in the glacierized catchments and diminished with decreasing glacier cover. The cation yields for the Grewingk (61%), Wosnesenski (36%), Halibut (23%), and Tutka (19%) were greater than the average from a compilation of glaciated streams (Torres et al., 2017), while the Jakolof (0%) had a lower cation yield than the global average for non-glacierized streams (Figure 5a). Similarly, the four glacierized catchments in our study region had higher mean runoff than the average for global glacierized

MUÑOZ ET AL. 14 of 24

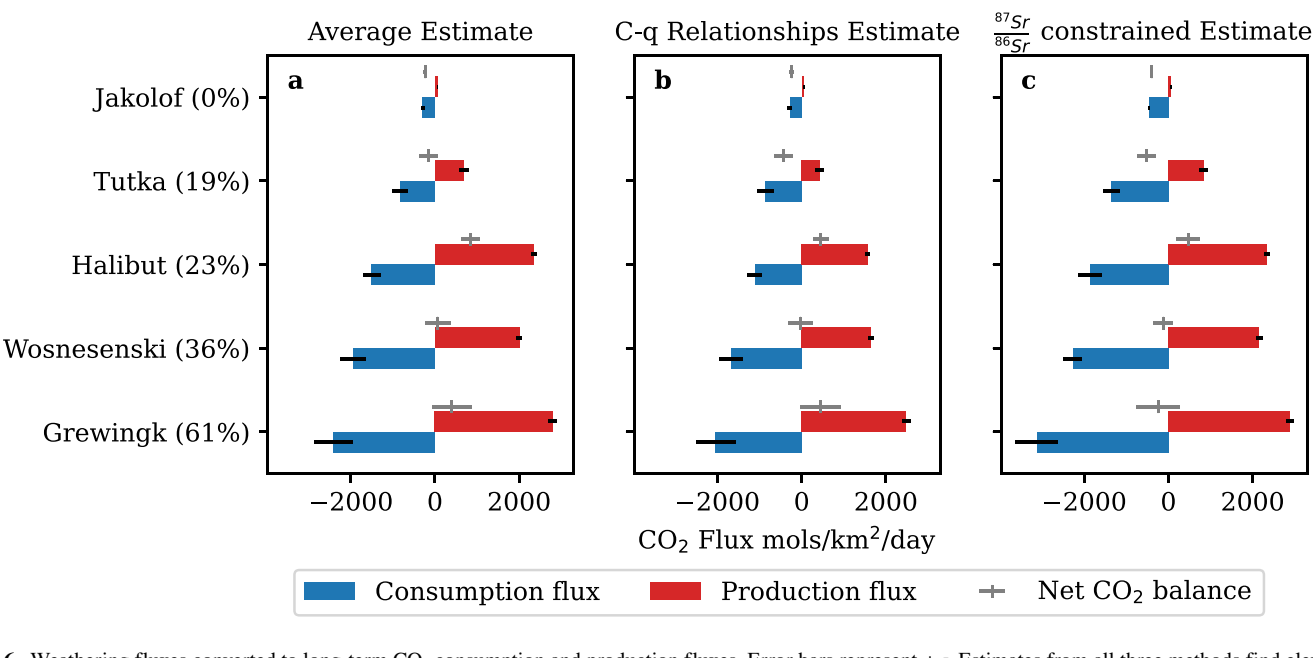


Figure 6. Weathering fluxes converted to long-term CO_2 consumption and production fluxes, Error bars represent $\pm \sigma$. Estimates from all three methods find elevated CO_2 production from pyrite oxidation in all glacierized catchments (a) CO_2 consumption and production fluxes calculated from average discharge and average. We find that above 23% glacial cover watersheds are a source or net neutral, while below 23% they are a net sink. (b) CO_2 consumption and production fluxes calculated from C-q relationships. Similar findings to a, with all fluxes being lower in magnitude. (c) CO_2 consumption and production fluxes calculated from average discharge and average concentration with 87 Sr/ 86 Sr isotopic constraints. Findings are similar to a but with greater consumption fluxes predicted which results in only the Halibut (23%) being a definitive source of CO_2 .

streams (Figure 5a). The Jakolof (0%) has a mean runoff (350 mm/yr) that is near the global average (298 mm/yr) for non-glacierized streams (Torres et al., 2017). The cation fluxes were attributed to each endmember utilizing the inversion $F_{\rm endmember}$ results and the stoichiometry in Equations 1–5 to compare $\rm CO_2$ fluxes associated with rock weathering from silicate carbonate and pyrite oxidation between catchments. Following the cation yields, weathering related fluxes are highest in the more glacierized catchments and diminish with decreasing glacier cover (Figure 5b). Catchments with greater glacier cover (Grewingk 61%, Wosnesenski 36%, Halibut 22%) have higher estimated $\rm CO_2$ consumption fluxes associated with silicate weathering and $\rm CO_2$ production associated with pyrite oxidation. The less glacierized catchments (Tutka 19%, Jakolof 0%) have lower consumption and production fluxes. The Tutka (19% cover) has much greater pyrite oxidation fluxes than the least glacierized catchment (Jakolof 0%). All catchments had higher carbonate than silicate weathering fluxes, with higher fluxes and increased pyrite oxidation fluxes corresponding to glacierized catchments and lower fluxes and decreased pyrite oxidation fluxes corresponding to less glacierized catchments (Figure 5b).

For the major ion inversion, we have sufficient data to estimate fluxes with Concentration-runoff (C-q) and fraction-runoff (F-q) relationships, which account for dilution and diminished flux estimations in glacierized catchments. Silicate, carbonate, and pyrite oxidation weathering fluxes are systematically higher when computed with averaged values and lower when allowing for dilution with C-q relationships (Figure 5b). These differences exist in all of our catchments but are more pronounced in the more glacierized catchments. We show differences in CO_2 fluxes in Figure 5b, and only report differences which are found to be significant using a one-tailed independent, two sample students T-test, with a p value < 0.05. The non-glacierized catchment has the smallest (24%) difference in flux estimates, which is only significant for the pyrite oxidation fluxes. The highest dilution effect is apparent in the Halibut (23%) glacier cover) with a 39% overestimation in silicate weathering fluxes, 39% overestimation in carbonate weathering fluxes, and 49% overestimation in pyrite oxidation fluxes when utilizing average versus C-q relationships. Predictions of fluxes with average runoff and concentration are higher than predictions utilizing C-q relationships, especially in glacierized catchments.

Comparing the average flux estimates from the major ion and isotopic inversion, we find that including ⁸⁷Sr/⁸⁶Sr isotopes in the inversion results in higher predicted fractions from silicate weathering (Figure 3b) and higher silicate weathering fluxes (Figure 6c). The 4% mean increase in solutes attributed to silicate weathering across

MUÑOZ ET AL. 15 of 24

Table 3Inorganic Weathering CO₂ Balances in mol/km²/Day Estimated With Average (Major Ion and Isotopic Inversion) and C-q (Major Ion Inversion Only) Estimation Methods

	Average: Majo	r ion inversion	C-q: Major io	n inversion	Average: Isotopic inversion	
Watershed	CO ₂ balance (mol/km²/day)	σ	CO ₂ balance (mol/km²/day)	σ	CO ₂ balance (mol/km ² /day)	σ
Jakolof (0%)	-232.59	39.233	-232.64	56.38	-392.04	24.87
Tutka (19%)	-143.39	216.50	-429.10	220.37	-516.86	218.94
Halibut (23%)	840.96	215.79	458.02	182.20	476.42	283.14
Wosnesenski (36%)	64.00	307.19	-28.45	289.09	-118.82	229.88
Grewingk (61%)	404.19	468.97	440.60	475.49	-247.53	514.79

catchment results in overall higher silicate weathering fluxes. The mean isotopic inversion silicate weathering ${\rm CO}_2$ flux is greater than the mean for the major ion inversion for all catchments when compared with a one-tailed independent, two sample students T-test (p values < 0.05). This change is more proportionally pronounced in non-glacierized catchments than in glacierized catchments, with mean fluxes being 65% larger in the Tutka (19% cover) and 57% greater in the Jakolof (0% cover). This difference is less pronounced in glacierized catchments due to greater overall fluxes with silicate weathering fluxes being 30% greater in the Grewingk (61% cover), 17% greater in the Wos (36% cover), and 23% greater in the Halibut (23% cover). The inorganic weathering ${\rm CO}_2$ balances for all three methods are presented in Table 3. The changes in silicate weathering fluxes between the average estimate for the major and isotopic inversions produce shifts that are statistically significant for the Grewingk (61% cover), and the Jakolof (0% cover) when comparing the mean ${\rm CO}_2$ balance with a one-tailed independent two sample students T-test (p values < 0.05). Although all methods are within σ of 0, silicate weathering fluxes for the isotopic inversion with the inclusion of ${}^{87}{\rm Sr}/{}^{86}{\rm Sr}$ isotopes resulted in the Grewingk's (61%) modeled mean ${\rm CO}_2$ weathering budget to change from positive to negative (Table 3, Figures 6c and 7b).

4. Discussion

4.1. C-q Analysis and Weathering Regime Implications

Our flux estimates with the major ion inversion utilizing average concentration and runoff overpredict fluxes at all glacierized sites when compared with the estimation using *C-q* relationships (Figure 5b). This finding is unsurprising given the clear dilution relationships (Figure 4) prevalent in our glacierized catchments. Other studies (e.g., Hindshaw et al., 2011) have reported similar departures from chemostatic behavior in glacierized watersheds. We find that even 19% glacierization (Halibut) results in increased dilution effects (Figure 5b), and overestimation of fluxes when utilizing the common assumption of chemostasis and average concentration and discharge (Bluth & Kump, 1994; Gaillardet et al., 1999; Gislason et al., 1996; Torres et al., 2017). In contrast, our least glacierized site exhibits the most chemostatic behavior, and is most suited to traditional estimation methods. As such, flux estimates that do not consider dilution effects will overpredict weathering related fluxes in glacierized catchments and other regions where chemostatic relationships are less prevalent.

Contrasting C-q and F-q behaviors between glacierized and non-glacierized catchments suggest that glacierization modulates the weathering regime of watersheds. Solute dilution across our glacierized catchments places them in a kinetically limited weathering regime, where mineral dissolution rates are unable to keep up with the steady supply of fresh material. This is supported by regional studies finding that glacierized catchments feeding the Gulf of Alaska transport more material in their suspended rather than dissolved load (Jenckes et al., 2022). Glacial melt discharged directly to a stream has lower reactive residence times than precipitation or snow infiltrating through the soil profile, and $F_{\rm endmember}$ contributions for carbonate and silicate remain constant across runoff for the more glacierized catchments, suggesting that fluid transit times remain below reaction rates (sensu Maher, 2011). Additionally, these kinetic limitations are likely due to cold temperatures suppressing reaction rates when comparing between similar catchments with different mean annual temperatures, which is detailed in the companion manuscript (Jenckes et al., 2024), and has been shown to be a mechanism controlling sedimentary rock oxidative pathways (Soulet et al., 2021). With decreasing glacierization, the river sources more water from longer flow paths with greater reactive residence times and reactions can proceed to completion, resulting

MUÑOZ ET AL. 16 of 24

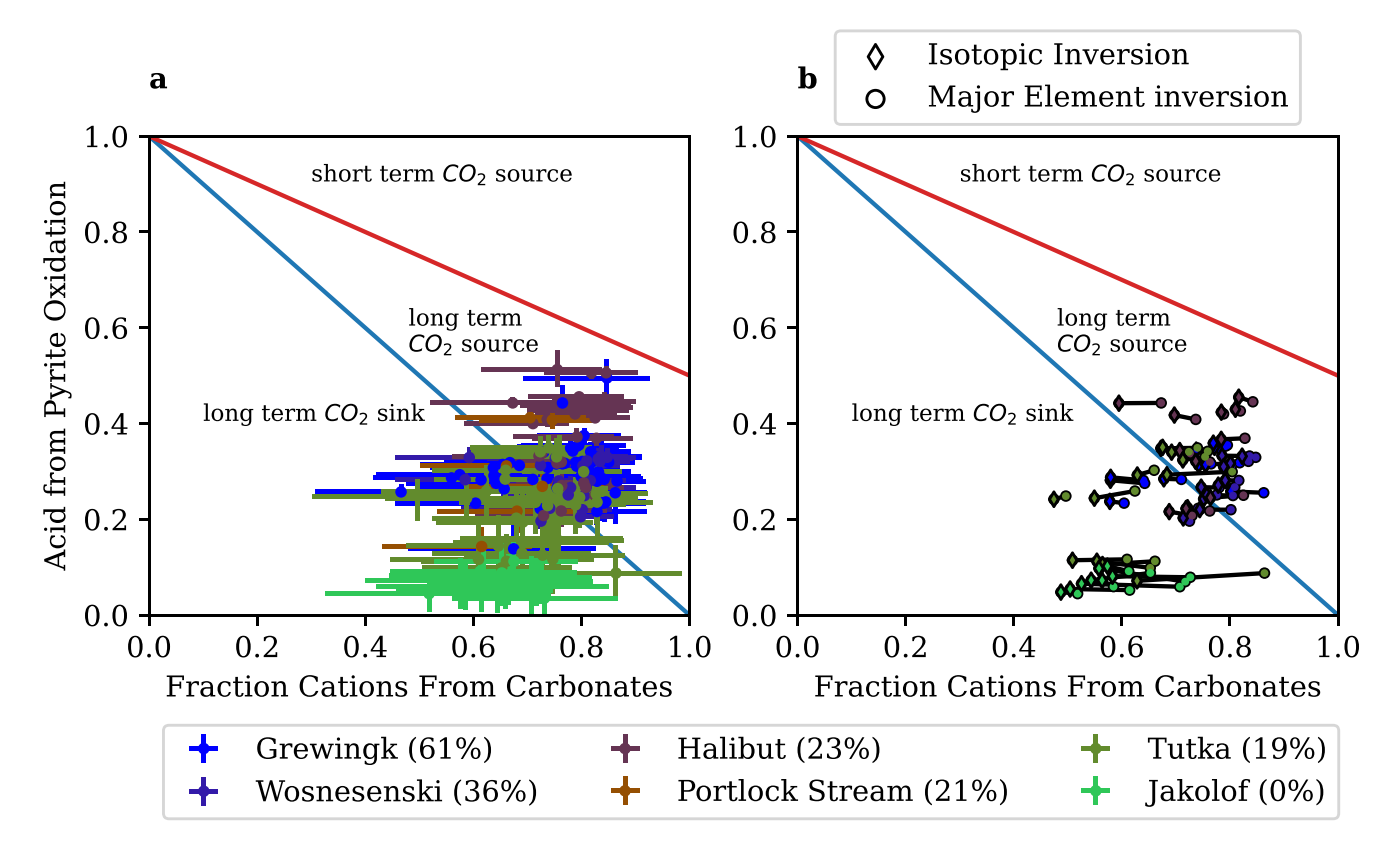


Figure 7. The inversion model predicted acid and cation sources and implications for the long-term carbon budget. Error bars represent the 25th and 75th percentiles of outputs. Red and blue lines are set by the stoichiometry of reactions shown in Equations 1-5 and link the acid and cation sources to the alk/DIC of the ocean and the pCO₂ of the atmosphere (Torres et al., 2016) (a) Major elemental inversion results. The non glacierized catchment is the only watershed where all samples and error plot under the 1:1 line indicating it is a long-term sink. The more glacierized catchments fall between being a sink and a long-term source. (b) Changes in output values shown for samples that were modeled with the addition of 87 Sr/ 86 Sr isotopic constraints. Sr isotopic inversions predict more contribution from silicates, and therefore points shift to the left.

in chemostatic and thermodynamically limited behavior of solutes. However, the fractional contributions from silicate weathering decrease at higher flows, indicating that there are still some kinetic limitations on silicate dissolution. Despite enhanced mineral supply and increased reactive surface area in glacierized catchments, direct discharge to the stream, and high runoff combine with temperature to impose kinetic limitations on weathering reactions. With the reduction in glacierization, sediment transport and supply decrease and water residence times increase, which transition the weathering regime from a kinetically limited regime where sediment supply outpaces reactions to a thermodynamically limited regime where reactions reach completion and export is limited by the availability of fresh material.

4.2. Catchment Characteristics Influence on Weathering

Multiple linear regression further demonstrates that changes in the weathering regime associated with glacier retreat are driven by landscape evolution. Other than minor differences in lithology, which are known to be the dominant controls on solute-generating weathering reactions at the global scale (Bluth & Kump, 1994; Gaillardet et al., 1999; Wymore et al., 2017), fractional contributions from silicate and carbonate endmembers both increase with increasing forest cover. The presence of forests can be thought of as a proxy for developed soils and an increase in the reaction time of water. The transition from highly glacierized to highly forested watersheds is accompanied by a shift in the weathering regime. As glaciers contribute less and a higher proportion of streamflow comes from infiltrating snow and precipitation, fluid reactive residence times increase, giving dissolution reactions the opportunity to reach equilibrium. As glaciers recede and the hydrology and landscapes adjust to non-glacierized conditions, catchment shift from being kinetically limited to approaching thermodynamic limitations. In these thermodynamically limited catchments, the rapid reaction kinetics of pyrite dissolution means that the pyrite is exhausted, and we see evidence of this in our reduced pyrite oxidative fluxes in two of our most

MUÑOZ ET AL. 17 of 24

deglaciated catchments. In addition, in our non-glacierized catchment, we see evidence for a reduced contribution from silicate weathering at high discharges, suggesting that higher discharge conditions result in shorter flowpath lengths (or faster volumetric flow rates) that result in kinetic limitations on silicate weathering. We observe a shift in regime from kinetically limited with high runoff and low water residence time to a thermodynamically limited regime with lower runoff and higher water residence times in our catchments. In sum, deglaciation changes the weathering regime and hydrology of catchments, which together are expressed in the overall weathering fluxes and the balance between silicate and carbonate weathering.

Our estimates suggest that greater weathering fluxes are primarily driven by high runoff in glacierized catchments (Figure 5), likely due to melt associated with warming. Previous workers have demonstrated that in glacierized catchments the highest overall flux of total dissolved solids occurs in months of peak glacier melt contribution (Jenckes et al., 2023). Here we extend these findings to primary weathering fluxes and show that their increase is driven by higher runoff despite measurable dilution patterns in the *C-q* relationships. Examining the differences between solute behavior and fractional contributions from weathering endmembers allows us to infer the landscape processes resulting in differences in water chemistry. In our more glacierized catchments, solutes are diluted as fractional contributions remain near constant. This is consistent with an unchanging supply of fresh reactive mineral surfaces and flowpath residence times being shorter than that required for equilibrium mineral dissolution. In contrast, less glacierized catchments see less dilution but higher variability in their fractional contributions. Together, the variability suggests that with a lower supply of fresh mineral surfaces in less glacierized catchments, flowpath variability between baseflow and peak runoff and varying transit times drive *C-q* and *F-q* relationships (Winnick et al., 2017). We find that runoff drives increased fluxes and watershed transition from being oversupplied with minerals to being constrained by thermodynamic limitations on weathering.

4.3. The Impact of Glacierization on Inorganic Weathering Related Carbon Balances

Figure 7 shows the proportion of carbonate weathering and weathering from sulfuric acid for each of the samples for the major ion (Figure 7a) and isotopic inversion (Figure 7b). The ratio of the contributions of these weathering products relates to the ratio of alkalinity and DIC of the ocean, which influence atmospheric pCO_2 , as outlined in Torres et al. (2016). The increase in silicate weathering contributions in the isotopic inversion is accommodated by a decrease in carbonate contributions, which shifts points to the left (Figure 7b) and causes some samples to switch from reflecting a long-term source to being a long-term sink. The impact of this switch propagates into the weathering fluxes (Figure 6) and indicates that the additional information gained by adding Sr isotopes in the isotopic inversion may have implications for CO_2 balances.

We quantify the net inorganic weathering related carbon balances (Figure 6, Table 3) in three ways: with average results from the major ion inversion (Figure 6a), with the C-q method and major ion inversion results (Figure 6b), and using average results from the isotopic average (Figure 6c). For the first three catchments ranging from 0% to 23% glacier cover, all three flux estimates (Major ion average Figure 6a, Major ion C-q Figure 6b, Isotopic average Figure 6c) agree on the sign (source or sink) of the inorganic weathering related CO₂ balances. The sign of the mean of the final two most glacierized catchments varies depending on the method used, but we note that all estimates fall within σ of neutral (Table 3, Figure 6). Both major ion flux estimations (average, C-q) suggest that within our glacier sequence, inorganic rock weathering reactions result in catchments with greater than 23% glacierization being neutral or net sources of CO₂ on timescales greater than ocean mixing (Figures 6a, 6b, and 7a, Table 3) (Zeebe & Wolf-Gladrow, 2001). Our three most glacierized catchments have high area normalized pyrite oxidation fluxes and silicate weathering fluxes, explaining the net production of CO2 in two out of the three more glacierized catchments. We expect that quantifying erosional and rock organic carbon oxidation fluxes would further add to the source term, while low soil cover in these catchments indicates that little would be added to the sink term. The silicate weathering fluxes remain elevated in the least glacierized catchments while pyrite oxidation tapers off, resulting in those catchments serving as CO₂ sinks. Due to similar reaction kinetics (Horan et al., 2017), we expect rock oxidation to follow similar patterns as the pyrite oxidation and not greatly modify the balance in our least glacierized catchments. Our findings demonstrate that using major ion inversions with average chemistry and discharge overpredicts weathering fluxes (Figure 5b), but both this and our updated C-q and F-q estimate agrees with previous findings that weathering in glacierized catchments serves as a source of CO2 (Torres et al., 2017). This agreement makes sense given the similar constraints utilized in their inversions compared to our major ion inversion. The Isotopic inversion adds ⁸⁷Sr/⁸⁶Sr isotopes as an inversion constraint and finds increased silicate weathering fluxes, suggesting a different overall balance.

MUÑOZ ET AL. 18 of 24

The inclusion of ⁸⁷Sr/⁸⁶Sr isotopes in the matrix inversions increases the mean silicate end member contributions and increases our estimates of silicate weathering fluxes. This is due to clear influence from the more depleted silicate ⁸⁷Sr/⁸⁶Sr in the river water samples and is shown in Figure S4 in Supporting Information S1. Only one of our watersheds (Halibut 23%) is a source of CO₂, with greatly enhanced silicate weathering fluxes balancing out pyrite oxidation in the more glacierized catchments, and diminished pyrite oxidation in the non-glacierized catchment. We find that adding more isotopic constraints predict enhanced silicate weathering fluxes in deglaciating catchments that may serve as CO₂ sinks over long timescales.

4.4. Glacier Retreat and Climate Feedbacks

Our findings suggest that the process of glacier retreat enhances all rock weathering but that kinetically slow silicate weathering persists beyond rapid pyrite oxidation and exhaustion, creating the potential for a negative feedback loop whereby decreased glacierization due to increased temperatures can decrease CO2 in the atmosphere. While we did not quantify rock organic carbon oxidation in this study, it has similar reaction kinetics and responds to similar forcings as pyrite oxidation (Horan et al., 2017), highlighting the need to quantify rock organic carbon oxidation and see if its reactions exhaust on similar timescales. Additionally, elevated silicate weathering has been attributed to increased soil organic carbon storage, and landscapes transitioning from ice to barren to forest cover will be associated with additional carbon drawdown not accounted for in our study (Klaar et al., 2015; Slessarev et al., 2022; Torres et al., 2020). We want to emphasize that these findings are restricted to catchments that are deglaciating. This is because we expect runoff to be higher in our catchments (and across glacierized catchments globally) because we are in a time period of increased warming and deglaciation of the high latitudes (Beamer et al., 2017; Bliss et al., 2014; Radić & Hock, 2014), and thus increased weathering fluxes and runoff are paired. However, with equivalent precipitation forcing, we would expect a catchment with increasing glacial cover to have lower runoff than one without any glacier cover, as increasing ice cover corresponds to an increase in storage and would delay runoff (Jansson et al., 2003). Additionally, the advancement of ice would cover landscapes which have already seen the development of soils and exhaustion of pyrite in the weathering zone, suggesting that there are different mechanisms at play when catchments are gaining or losing glacier cover. Because of this, our findings are inconclusive with regard to the growth of glaciers and the hypothesis that glaciation serves as a negative feedback whereby increased glacier cover produces CO₂ and prevents runaway glaciation (e.g., Torres et al., 2017). We make this distinction because the increase in runoff drives our elevated weathering fluxes, and this increased runoff is produced by glacier loss (Beamer et al., 2017). To definitively assess the potential for glaciation to serve as a self-regulating negative feedback via pyrite oxidation, catchments with increasing glacier cover as the climate warms and atmospheric CO₂ increase should be investigated.

5. Conclusions

5.1. Runoff Drives Solute Export Despite Dilution

Our findings support the hypothesis that glacierized catchments have higher weathering fluxes than non-glacierized catchments. These patterns exist despite our analysis of concentration discharge relationships finding clear dilution patterns. Together, this suggests that not accounting for dilution likely overestimates flux contributions in glacierized catchments. We note that an additional source of overestimation could come from the sampling bias associated with the difficulties of conducting fieldwork in the winter in glacierized catchments. The most complete compilation to date of the hydrochemistry of glacierized catchments (Torres et al., 2017) contains the findings of ~50 studies spanning 95 sites. Of those 95 sites, only 52 sites have a record of discharge and of those 52, only 26 record measurements made outside the primary ablation season. Our study limited this seasonal bias by extending measurements into the spring and fall, but we are still sample limited in the winter months. While glacierized streams often freeze over in the winter, and thus the majority of solute fluxes are captured by these studies, the extension of the ablation discharge conditions to annual average surely overestimated the runoff and flux contributions from glacierized catchments. With these limitations in mind, our findings support previous findings by Torres et al. (2017) and Anderson et al. (2000) that increased runoff in glacierized catchment results in increased solute and weathering fluxes, despite our observation of dilution. However, we note that glacierized catchments are likely to have higher runoff compared to non-glacierized catchments in today's warming, deglaciating world, but that runoff and fluxes may be lower in times where glaciers are advancing and thus increasing watershed storage (Jansson et al., 2003).

MUÑOZ ET AL. 19 of 24

5.2. Glacierization Alters the Weathering Regime of Catchments

We find that glaciers alter the weathering regime in deglaciating catchments by increasing runoff and modifying the landscape. In tandem, we suggest that these hydrologic and geomorphic changes affect the reactive residence time of water as well as the supply of minerals and the flow path water takes through the catchment. Our findings demonstrate some kinetic limitations on all weathering reactions in glacierized catchments consistent with the hypothesis that an overabundance of minerals produced by enhanced physical erosion due to glaciation is combined with lower reactive residence times from glacial melt discharging directly to the stream. As glaciers recede and the catchment shifts to increasing forest cover, we find more chemostatic relationships consistent with increased fluid residence times which we attribute to increased landscape stability and the influence of rooting plants. Together, our analyses of weathering fluxes and concentration discharge relationships paired with landscape analysis demonstrate how deglaciation impacts the weathering regime of catchments by modifying their hydrology and landscape evolution. This highlights the importance of catchment-specific work where fluxes are compared over similar landscapes that principally differ in a single landscape feature (in our case the features associated with glacierization).

5.3. Weathering CO₂ Balances and Global Carbon Cycle Implications

We calculated inorganic CO₂ balances due to weathering reactions in our glacial sequence by partitioning the above average weathering fluxes into endmember contributions. We found lower contributions from pyrite oxidation and high residual silicate weathering contributions in less glacierized catchments. We expect that the inclusion of rock organic carbon oxidation would match this trend due to similar reaction kinetics. In more glacierized catchments, pyrite oxidation paired with carbonate weathering outpaces CO₂ drawdown from silicate weathering (and may result in catchments being a source of CO₂ if considering additional sources such as petrogenic carbon oxidation; cf. Hilton & West, 2020). At low and no glacial cover, silicate weathering outpaces pyrite oxidation and results in deglacierized or low glacier cover catchments serving as a carbon sink. These relationships support the hypothesis that the process of deglaciation may serve as a negative feedback loop (e.g., Kump et al., 1999), whereby decreasing glacier cover results in elevated silicate weathering. Additionally, since high runoff due to glacier loss drives increased solute fluxes, we emphasize that with increased glaciation, decreased runoff implies that weathering related carbon fluxes diminish (e.g., Gislason et al., 1996; Kump et al., 1999).

Data Availability Statement

The hydrochemistry data used in this study were published in Jenckes et al. (2023) The MEANDIR model code (version 1.2) is available at github.com/PrestonCosslettKemeny/MEANDIR. The rock data utilized to constrain the inversions and the ⁸⁷Sr/⁸⁶Sr measurements of river water are presented in sd01.xlsx and sd02.xlsx (Data Sets S1 and S2), respectively.

References

Anderson, S. P., Drever, J. I., Frost, C. D., & Holden, P. (2000). Chemical weathering in the foreland of a retreating glacier. *Geochimica et Cosmochimica Acta*, 64(7), 1173–1189. https://doi.org/10.1016/s0016-7037(99)00358-0

Archer, D. (2005). Fate of fossil fuel CO₂ in geologic time. *Journal of Geophysical Research*, 110(C9), C09S05. https://doi. org/10.1029/2004jc002625

Beamer, J. P., Hill, D. F., Arendt, A., & Liston, G. E. (2016). High-resolution modeling of coastal freshwater discharge and glacier mass balance in the Gulf of Alaska watershed. Water Resources Research, 52(5), 3888–3909. https://doi.org/10.1002/2015wr018457

Beamer, J. P., Hill, D. F., Mcgrath, D., Arendt, A., & Kienholz, C. (2017). Hydrologic impacts of changes in climate and glacier extent in the Gulf of Alaska watershed. Water Resources Research, 53(9), 7502–7520. https://doi.org/10.1002/2016wr020033

Benn, D., & Evans, D. J. (2010). Glaciers and glaciation (2nd ed.). Routledge.

Berner, R. A., Lasaga, A. C., & Garrels, R. M. (1983). Carbonate-silicate geochemical cycle and its effect on atmospheric carbon dioxide over the past 100 million years. *American Journal of Science*, 283(7), 641–683. Article 7. https://doi.org/10.2475/ajs.283.7.641

Bivand, R. (2023). rgrass7: Interface between "GRASS" geographical information system and "R" (0.2-10) [Computer software]. CRAN. Retrieved from https://CRAN.R-project.org/package=rgrass7

Bliss, A., Hock, R., & Radić, V. (2014). Global response of glacier runoff to twenty-first century climate change. *Journal of Geophysical Research: Earth Surface*, 119(4), 717–730. Article 4. https://doi.org/10.1002/2013jf002931

Bluth, G. J., & Kump, L. R. (1994). Lithologic and climatologic controls of river chemistry. Geochimica et Cosmochimica Acta, 58(10), 2341–2359. https://doi.org/10.1016/0016-7037(94)90015-9

Bouchez, J., Moquet, J.-S., Espinoza, J. C., Martinez, J.-M., Guyot, J.-L., Lagane, C., et al. (2017). River mixing in the Amazon as a driver of concentration-discharge relationships. *Water Resources Research*, 53(11), 8660–8685. https://doi.org/10.1002/2017wr020591

MUÑOZ ET AL.

program.

Acknowledgments

We would like to thank Bob Hilton and two anonymous reviewers for feedback

that greatly improved the quality of this manuscript. We would also like to thank

Laurence Smith and Preston Kemeny for

supported by Alaska EPSCoR NSF award

OIA-1757347 and the state of Alaska.

Muñoz acknowledges support from the

Graduate Research Fellowships Program

(GRFP), The Brown University Presiden-

tial Fellowship, and the Institute at Brown for Environment and Society (IBES)

Grant. Ramos acknowledges support from

edges support from the Sloan Indigenous Graduate Partnership Fellowship and the

Aleut Foundation Graduate Scholarship

Graduate Research Travel & Training

NSF-EAR-2053056. Jenckes acknowl-

National Science Foundation (NSF)

discussions which aided the progression of this work. This research was

- Bufe, A., Hovius, N., Emberson, R., Rugenstein, J. K., Galy, A., Hassenruck-Gudipati, H. J., & Chang, J.-M. (2021). Co-variation of silicate, carbonate and sulfide weathering drives CO₂ release with erosion. *Nature Geoscience*, 14(4), 211–216. https://doi.org/10.1038/s41561-021-00714-3
- Burke, A., Present, T. M., Paris, G., Rae, E. C., Sandilands, B. H., Gaillardet, J., et al. (2018). Sulfur isotopes in rivers: Insights into global weathering budgets, pyrite oxidation, and the modern sulfur cycle. *Earth and Planetary Science Letters*, 496, 168–177. https://doi.org/10.1016/j.epsl.2018.05.022
- Calmels, D., Gaillardet, J., Brenot, A., & France-Lanord, C. (2007). Sustained sulfide oxidation by physical erosion processes in the Mackenzie River basin: Climatic perspectives. *Geology*, 35(11), 1003–1006. https://doi.org/10.1130/g24132a.1
- Chamberlain, C. P., Waldbauer, J. R., & Jacobson, A. D. (2005). Strontium, hydrothermal systems and steady-state chemical weathering in active mountain belts. Earth and Planetary Science Letters, 238(3–4), 351–366. https://doi.org/10.1016/j.epsl.2005.08.005
- Chaudhuri, S., Clauer, N., & Semhi, K. (2007). Plant decay as a major control of river dissolved potassium: A first estimate. Chemical Geology, 243(1–2), 178–190. https://doi.org/10.1016/j.chemgeo.2007.05.023
- Chen, J., Montañez, I. P., Qi, Y., Shen, S., & Wang, X. (2018). Strontium and carbon isotopic evidence for decoupling of pCO₂ from continental weathering at the apex of the late Paleozoic glaciation. *Geology*, 46(5), 395–398. https://doi.org/10.1130/g40093.1
- Clark, S. H. B. (1973). The McHugh complex of South-Central Alaska (contributions to stratigraphy 1372-D; geologic Survey bulletin). United States Department of the Interior and United States Geological Survey.
- Clow, D. W., & Mast, M. A. (2010). Mechanisms for chemostatic behavior in catchments: Implications for CO₂ consumption by mineral weathering. Chemical Geology, 269(1–2), 40–51. https://doi.org/10.1016/j.chemgeo.2009.09.014
- Cole, T. L., Torres, M. A., & Kemeny, P. C. (2022). The hydrochemical signature of incongruent weathering in Iceland. *Journal of Geophysical Research: Earth Surface*, 127(6), e2021JF006450, https://doi.org/10.1029/2021jf006450
- Connelly, W. (1978). Uyak complex, Kodiak Islands, Alaska: A Cretaceous subduction complex. *Geological Society of America Bulletin*, 89(5),
- 755–769. https://doi.org/10.1130/0016-7606(1978)89<755:uckiaa>2.0.co;2
 Derry, L. A., Kurtz, A. C., Ziegler, K., & Chadwick, O. A. (2005). Biological control of terrestrial silica cycling and export fluxes to watersheds.
- Nature, 433(7027), 728–731. https://doi.org/10.1038/nature03299

 Dewitz, J., & U.S. Geological Survey. (2020). National land cover database (NLCD) 2016 (2.0) [Dataset]. U.S. Geological Survey data release.
- https://doi.org/10.5066/P96HHBIE
 Fountain, A. G., & Tangborn, W. V. (1985). Techniques for prediction of runoff from glacierized areas: Overview of contemporary techniques
- (pp. 27–41). IAHS-AISH Publication.
- Gabet, E. J., & Mudd, S. M. (2009). A theoretical model coupling chemical weathering rates with denudation rates. *Geology*, 37(2), 151–154. https://doi.org/10.1130/g25270a.1
- Gaillardet, J., Dupré, B., Louvat, P., & Allègre, C. J. (1999). Global silicate weathering and CO₂ consumption rates deduced from the chemistry of large rivers. *Chemical Geology*, 159(1), 3–30. https://doi.org/10.1016/S0009-2541(99)00031-5
- Galy, A., France-Lanord, C., & Derry, L. A. (1999). The strontium isotopic budget of Himalayan Rivers in Nepal and Bangladesh. Geochimica et Cosmochimica Acta, 63(13–14), 1905–1925. https://doi.org/10.1016/s0016-7037(99)00081-2
- Gao, Y., Ma, M., Yang, T., Chen, W., & Yang, T. (2018). Global atmospheric sulfur deposition and associated impaction on nitrogen cycling in ecosystems. *Journal of Cleaner Production*, 195, 1–9. https://doi.org/10.1016/j.jclepro.2018.05.166
- Geilert, S., Grasse, P., Wallmann, K., Liebetrau, V., & Menzies, C. D. (2020). Serpentine alteration as source of high dissolved silicon and elevated 8³⁰Si values to the marine Si cycle. *Nature Communications*, 11(1), 5123. https://doi.org/10.1038/s41467-020-18804-y
- Gislason, S. R., Arnórsson, S., & Armannsson, H. (1996). Chemical weathering of basalt in Southwest Iceland; effects of runoff, age of rocks and vegetative/glacial cover. *American Journal of Science*, 296(8), 837–907. https://doi.org/10.2475/ajs.296.8.837
- Gleick, P. H. (1987). Regional hydrologic consequences of increases in atmospheric CO₂ and other trace gases. Climatic Change, 10(2), 137–160. https://doi.org/10.1007/bf00140252
- Godsey, S. E., Kirchner, J. W., & Clow, D. W. (2009). Concentration–discharge relationships reflect chemostatic characteristics of US catchments. Hydrological Processes, 23(13), 1844–1864. https://doi.org/10.1002/hyp.7315
- Hall, F. R. (1970). Dissolved solids discharge relationships: 1. Mixing models. Water Resources Research, 6(3), 845–850. https://doi.org/10.1029/wr006i003p00845
- Hemingway, J. D., Olson, H., Turchyn, A. V., Tipper, E. T., Bickle, M. J., & Johnston, D. T. (2020). Triple oxygen isotope insight into terrestrial pyrite oxidation. *Proceedings of the National Academy of Sciences of the United States of America*, 117(14), 7650–7657. https://doi.org/10.1073/pnas.1917518117
- Herman, F., & Braun, J. (2008). Evolution of the glacial landscape of the Southern Alps of New Zealand: Insights from a glacial erosion model. Journal of Geophysical Research, 113(F2), F02009. https://doi.org/10.1029/2007jf000807
- Hilton, R. G., & West, A. J. (2020). Mountains, erosion and the carbon cycle. Nature Reviews Earth & Environment, 1(6), 284–299. https://doi.org/10.1038/s43017-020-0058-6
- Hindshaw, R. S., Tipper, E. T., Reynolds, B. C., Lemarchand, E., Wiederhold, J. G., Magnusson, J., et al. (2011). Hydrological control of stream water chemistry in a glacial catchment (Damma Glacier, Switzerland). Chemical Geology, 285(1–4), 215–230. https://doi.org/10.1016/j.chemgeo.2011.04.012
- Hönisch, B., Ridgwell, A., Schmidt, D. N., Thomas, E., Gibbs, S. J., Sluijs, A., et al. (2012). The geological record of ocean acidification. *Science*, 335(6072), 1058–1063. https://doi.org/10.1126/science.1208277
- Hood, E., Battin, T. J., Fellman, J., O'neel, S., & Spencer, R. G. (2015). Storage and release of organic carbon from glaciers and ice sheets. *Nature Geoscience*, 8(2), 91–96. https://doi.org/10.1038/ngeo2331
- Hood, E., Fellman, J., Spencer, R. G., Hernes, P. J., Edwards, R., D'Amore, D., & Scott, D. (2009). Glaciers as a source of ancient and labile organic matter to the marine environment. *Nature*, 462(7276), 1044–1047. https://doi.org/10.1038/nature08580
- Horan, K., Hilton, R. G., Selby, D., Ottley, C. J., Gröcke, D. R., Hicks, M., & Burton, K. W. (2017). Mountain glaciation drives rapid oxidation of rock-bound organic carbon. Science Advances, 3(10), e1701107. https://doi.org/10.1126/sciadv.1701107
- Huss, M., Bookhagen, B., Huggel, C., Jacobsen, D., Bradley, R. S., Clague, J. J., et al. (2017). Toward mountains without permanent snow and ice. *Earth's Future*, 5(5), 418–435. https://doi.org/10.1002/2016EF000514
- Huss, M., & Hock, R. (2018). Global-scale hydrological response to future glacier mass loss. Nature Climate Change, 8(2), 135–140. https://doi.org/10.1038/s41558-017-0049-x
- Ibarra, D. E., Caves, J. K., Moon, S., Thomas, D. L., Hartmann, J., Chamberlain, C. P., & Maher, K. (2016). Differential weathering of basaltic and granitic catchments from concentration—discharge relationships. Geochimica et Cosmochimica Acta, 190, 265–293. https://doi.org/10.1016/j.gca.2016.07.006

MUÑOZ ET AL. 21 of 24

- Ibarra, D. E., Moon, S., Caves, J. K., Chamberlain, C. P., & Maher, K. (2017). Concentration—discharge patterns of weathering products from global rivers. Acta Geochimica, 36(3), 405–409. https://doi.org/10.1007/s11631-017-0177-z
- Idso, S. B., Balling, R. C., & Cerveny, R. S. (1990). Carbon dioxide and hurricanes: Implications of Northern Hemispheric warming for Atlantic/ Caribbean storms. Meteorology and Atmospheric Physics. 42(3-4), 259–263. https://doi.org/10.1007/bf01314829
- Immerzeel, W. W., Van Beek, L. P., & Bierkens, M. F. (2010). Climate change will affect the Asian water towers. Science, 328(5984), 1382–1385. https://doi.org/10.1126/science.1183188
- IPCC. (2014). In Climate change 2014: Synthesis report. Contribution of working groups I, II and III to the fifth assessment report of the intergovernmental panel on climate change. (AR5) IPCC. Retrieved from https://www.ipcc.ch/report/ar5/syr/
- Jacobson, A. D., Blum, J. D., & Walter, L. M. (2002). Reconciling the elemental and Sr isotope composition of Himalayan weathering fluxes: Insights from the carbonate geochemistry of stream waters. Geochimica et Cosmochimica Acta, 66(19), 3417–3429. https://doi.org/10.1016/s0016-7037(02)00951-1
- Jansson, P., Hock, R., & Schneider, T. (2003). The concept of glacier storage: A review. Journal of Hydrology, 282(1-4), 116-129. https://doi.org/10.1016/s0022-1694(03)00258-0
- Jenckes, J., Ibarra, D. E., & Munk, L. A. (2022). Concentration-discharge patterns across the Gulf of Alaska reveal geomorphological and glacierization controls on stream water solute generation and export. Geophysical Research Letters, 49(1), e2021GL095152. https://doi. org/10.1029/2021gl095152
- Jenckes, J., Munk, L., Ibarra, D., Boutt, D., Fellman, J., & Hood, E. (2023). Hydroclimate drives seasonal riverine export across a gradient of glacierized high-latitude coastal catchments. Water Resources Research, 59(4), e2022WR033305. https://doi.org/10.1029/2022wr033305
- Jenckes, J., Muñoz, S., Ibarra, D. E., Boutt, D. F., Munk, L.A. (2024). Geochemical weathering variability in high latitude watersheds of the Gulf of Alaska. *Journal of Geophysical Research: Earth Surface*. https://doi.org/10.1029/2023JF007284
- Kasting, J. F., & Catling, D. (2003). Evolution of a habitable planet. Annual Review of Astronomy and Astrophysics, 41(1), 429–463. https://doi.org/10.1146/annurev.astro.41.071601.170049
- Kattwinkel, M., Szöcs, E., Peterson, E., & Schäfer, R. B. (2020). Preparing GIS data for analysis of stream monitoring data: The R package openSTARS, PLoS One. 15(9), e0239237, https://doi.org/10.1371/journal.pone.0239237
- Kemeny, P. C., Lopez, G. I., Dalleska, N. F., Torres, M., Burke, A., Bhatt, M. P., et al. (2021). Sulfate sulfur isotopes and major ion chemistry reveal that pyrite oxidation counteracts CO₂ drawdown from silicate weathering in the Langtang-Trisuli-Narayani River system, Nepal Himalaya. Geochimica et Cosmochimica Acta, 294, 43–69. https://doi.org/10.1016/j.gca.2020.11.009
- Kemeny, P. C., & Torres, M. A. (2021). Presentation and applications of mixing elements and dissolved isotopes in rivers (MEANDIR), a custom-izable MATLAB model for Monte Carlo inversion of dissolved river chemistry. American Journal of Science, 321(5), 579–642. https://doi.org/10.2475/05.2021.03
- Klaar, M. J., Kidd, C., Malone, E., Bartlett, R., Pinay, G., Chapin, F. S., & Milner, A. (2015). Vegetation succession in deglaciated land-scapes: Implications for sediment and landscape stability. Earth Surface Processes and Landforms, 40(8), 1088–1100. https://doi.org/10.1002/esp.3691
- Kump, L. R., Arthur, M., Patzkowsky, M., Gibbs, M., Pinkus, D., & Sheehan, P. (1999). A weathering hypothesis for glaciation at high atmospheric pCO₂ during the Late Ordovician. *Palaeogeography, Palaeoclimatology, Palaeoecology*, 152(1–2), 173–187. https://doi.org/10.1016/s0031-0182(99)00046-2
- Kump, L. R., Brantley, S. L., & Arthur, M. A. (2000). Chemical weathering, atmospheric CO₂, and climate. Annual Review of Earth and Planetary Sciences, 28(1), 611–667. https://doi.org/10.1146/annurev.earth.28.1.611
- Lebrato, M., Garbe-Schönberg, D., Müller, M. N., Blanco-Ameijeiras, S., Feely, R. A., Lorenzoni, L., et al. (2020). Global variability in seawater Mg: Ca and Sr: Ca ratios in the modern ocean. *Proceedings of the National Academy of Sciences*, 117(36), 22281–22292. https://doi.org/10.1073/pnas.1918943117
- Lerman, A., Wu, L., & Mackenzie, F. T. (2007). CO₂ and H2SO4 consumption in weathering and material transport to the ocean, and their role in the global carbon balance. *Marine Chemistry*, 106(1–2), 326–350. https://doi.org/10.1016/j.marchem.2006.04.004
- Loper, D. (2009). Earth's habitable loop: Water, atmospheric structure, the geomagnetic field and plate tectonics. Acta Geodaetica et Geophysica Hungarica, 44(3), 265–269. https://doi.org/10.1556/ageod.44.2009.3.2
- Lovelock, J. E., & Watson, A. J. (1982). The regulation of carbon dioxide and climate: Gaia or geochemistry. *Planetary and Space Science*, 30(8), 795–802. https://doi.org/10.1016/0032-0633(82)90112-x
- Maher, K. (2011). The role of fluid residence time and topographic scales in determining chemical fluxes from landscapes. Earth and Planetary Science Letters, 312(1), 48–58. https://doi.org/10.1016/j.epsl.2011.09.040
- Maher, K., & Chamberlain, C. P. (2014). Hydrologic regulation of chemical weathering and the geologic carbon cycle. *Science*, 343(6178), 1502–1504. https://doi.org/10.1126/science.1250770
- Mallick, S., Kuhl, S. E., Saal, A. E., Klein, E. M., Bach, W., Monteleone, B. D., & Boesenberg, J. S. (2023). Evidence of South American lithosphere mantle beneath the Chile mid-ocean ridge. Earth and Planetary Science Letters, 620, 118320. https://doi.org/10.1016/j.epsl.2023.118320
- Millot, R., Gaillardet, J., Dupré, B., & Allègre, C. J. (2003). Northern latitude chemical weathering rates: Clues from the Mackenzie river basin, Canada. *Geochimica et Cosmochimica Acta*, 67(7), 1305–1329. https://doi.org/10.1016/s0016-7037(02)01207-3
- Milner, A. M., Khamis, K., Battin, T. J., Brittain, J. E., Barrand, N. E., Füreder, L., et al. (2017). Glacier shrinkage driving global changes in downstream systems. Proceedings of the National Academy of Sciences of the United States of America, 114(37), 9770–9778. https://doi. org/10.1073/pnas.1619807114
- Moon, S., Chamberlain, C. P., & Hilley, G. E. (2014). New estimates of silicate weathering rates and their uncertainties in global rivers. *Geochimica et Cosmochimica Acta*, 134, 257–274. https://doi.org/10.1016/j.gca.2014.02.033
- Moore, J., Jacobson, A. D., Holmden, C., & Craw, D. (2013). Tracking the relationship between mountain uplift, silicate weathering, and long-term CO₂ consumption with Ca isotopes: Southern Alps, New Zealand. Chemical Geology, 341, 110–127. https://doi.org/10.1016/j.chemgeo.2013.01.005
- Morcos, S. A. (1970). Chemical composition of seawater and the variation of calcium and alkalinity. *ICES Journal of Marine Science*, 33(2), 126–133. https://doi.org/10.1093/icesjms/33.2.126
- Nagorski, S. A., Kaspari, S. D., Hood, E., Fellman, J. B., & Skiles, S. M. (2019). Radiative forcing by dust and black carbon on the Juneau Icefield, Alaska. *Journal of Geophysical Research: Atmospheres*, 124(7), 3943–3959. https://doi.org/10.1029/2018jd029411
- National Atmospheric Deposition Program (NRSP-3). (2022). National atmospheric deposition program (NRSP-3) [Dataset]. NADP Program Office. Retrieved from https://nadp.slh.wisc.edu/precipitation/
- Négrel, P., Allègre, C. J., Dupré, B., & Lewin, E. (1993). Erosion sources determined by inversion of major and trace element ratios and strontium isotopic ratios in river water: The Congo Basin case. Earth and Planetary Science Letters, 120(1-2), 59-76. https://doi.org/10.1016/0012-821x(93)90023-3

MUÑOZ ET AL. 22 of 24

- Nicholson, A. E. (2019). What mechanisms have produced a self-regulating Earth system? Doctoral Thesis. University of Exeter.
- Pittock, A. B., & Salinger, M. J. (1982). Towards regional scenarios for a CO₂-warmed earth. Climatic Change, 4, 23-40.
- Pritchard, H. D. (2017). Asia's glaciers are a regionally important buffer against drought. Nature, 545(7653), 169–174. https://doi.org/10.1038/nature22062
- Quay, P. D., Wilbur, D., Richey, J. E., Devol, A. H., Benner, R., & Forsberg, B. R. (1995). The ¹⁸O: ¹⁶O of dissolved oxygen in rivers and lakes in the Amazon basin: Determining the ratio of respiration to photosynthesis rates in freshwaters. *Limnology & Oceanography*, 40(4), 718–729. https://doi.org/10.4319/lo.1995.40.4.0718
- Radić, V., & Hock, R. (2011). Regionally differentiated contribution of mountain glaciers and ice caps to future sea-level rise. *Nature Geoscience*, 4(2), 91–94. Article 2. https://doi.org/10.1038/ngeo1052
- Radić, V., & Hock, R. (2014). Glaciers in the Earth's hydrological cycle: Assessments of glacier mass and runoff changes on global and regional scales. Surveys in Geophysics, 35(3), 813–837. https://doi.org/10.1007/s10712-013-9262-y
- Raven, J., Caldeira, K., Elderfield, H., Hoegh-Guldberg, O., Liss, P., Riebesell, U., et al. (2005). Ocean acidification due to increasing atmospheric carbon dioxide. The Royal Society.
- Raymond, P. A., Hartmann, J., Lauerwald, R., Sobek, S., McDonald, C., Hoover, M., et al. (2013). Global carbon dioxide emissions from inland waters. *Nature*, 503(7476), 355–359. https://doi.org/10.1038/nature12760
- R Core Team. (2023). R: A language and environment for statistical computing. R Foundation for Statistical Computing. Retrieved from https://
- Riebe, C. S., Kirchner, J. W., & Finkel, R. C. (2004). Erosional and climatic effects on long-term chemical weathering rates in granitic landscapes spanning diverse climate regimes. *Earth and Planetary Science Letters*, 224(3–4), 547–562. https://doi.org/10.1016/j.epsl.2004.05.019
- Salmon-Monviola, J., Moreau, P., Benhamou, C., Durand, P., Merot, P., Oehler, F., & Gascuel- Odoux, C. (2013). Effect of climate change and increased atmospheric CO₂ on hydrological and nitrogen cycling in an intensive agricultural headwater catchment in western France. Climatic Change, 120(1–2), 433–447. https://doi.org/10.1007/s10584-013-0828-y
- Schäfer, K. V., Oren, R., Lai, C.-T., & Katul, G. G. (2002). Hydrologic balance in an intact temperate forest ecosystem under ambient and elevated atmospheric CO₂ concentration. *Global Change Biology*, 8(9), 895–911. https://doi.org/10.1046/j.1365-2486.2002.00513.x
- atmospheric CO₂ concentration. *Global Change Biology*, 8(9), 895–911. https://doi.org/10.1046/j.1363-2486.2002.00513.x Schneider, S. H. (1984). On the empirical verification of model-predicted CO₂-induced climatic effects. *Climate Processes and Climate Sensitivity*, 29, 187–201. https://doi.org/10.1029/gm029p0187
- Schopka, H., Derry, L., & Arcilla, C. (2011). Chemical weathering, river geochemistry and atmospheric carbon fluxes from volcanic and ultramafic regions on Luzon Island, the Philippines. *Geochimica et Cosmochimica Acta*, 75(4), 978–1002. https://doi.org/10.1016/j.gca.2010.11.014
- Seabold, S., & Perktold, J. (2010). Statsmodels: Econometric and statistical modeling with python. Proceedings of the 9th Python in Science Conference, 57(61), 10–25080.
- Slessarev, E. W., Chadwick, O. A., Sokol, N. W., Nuccio, E. E., & Pett-Ridge, J. (2022). Rock weathering controls the potential for soil carbon storage at a continental scale. *Biogeochemistry*, 157(1), 1–13. https://doi.org/10.1007/s10533-021-00859-8
- Soulet, G., Hilton, R. G., Garnett, M. H., Roylands, T., Klotz, S., Croissant, T., et al. (2021). Temperature control on CO₂ emissions from the weathering of sedimentary rocks. *Nature Geoscience*, 14(9), 665–671. https://doi.org/10.1038/s41561-021-00805-1
- Stallard, R. F. (1998). Terrestrial sedimentation and the carbon cycle: Coupling weathering and erosion to carbon burial. *Global Biogeochemical Cycles*, 12(2), 231–257. https://doi.org/10.1029/98gb00741
- Tipper, E. T., Bickle, M. J., Galy, A., West, A. J., Pomiès, C., & Chapman, H. J. (2006). The short term climatic sensitivity of carbonate and silicate weathering fluxes: Insight from seasonal variations in river chemistry. *Geochimica et Cosmochimica Acta*, 70(11), 2737–2754. https://doi.org/10.1016/j.gca.2006.03.005
- Torres, M. A., Kemeny, P. C., Lamb, M. P., Cole, T. L., & Fischer, W. W. (2020). Long-term storage and age-biased export of fluvial organic carbon: Field evidence from West Iceland. *Geochemistry*, *Geophysics*, *Geosystems*, 21(4), e2019GC008632. https://doi.org/10.1029/2019GC008632
- Torres, M. A., Moosdorf, N., Hartmann, J., Adkins, J. F., & West, A. J. (2017). Glacial weathering, sulfide oxidation, and global carbon cycle feedbacks. Proceedings of the National Academy of Sciences of the United States of America, 114(33), 8716–8721. https://doi.org/10.1073/pnas.1702953114
- Torres, M. A., West, A. J., & Clark, K. E. (2015). Geomorphic regime modulates hydrologic control of chemical weathering in the Andes–Amazon. Geochimica et Cosmochimica Acta, 166, 105–128. https://doi.org/10.1016/j.gca.2015.06.007
- Torres, M. A., West, A. J., Clark, K. E., Paris, G., Bouchez, J., Ponton, C., et al. (2016). The acid and alkalinity budgets of weathering in the Andes–Amazon system: Insights into the erosional control of global biogeochemical cycles. *Earth and Planetary Science Letters*, 450, 381–391. https://doi.org/10.1016/j.epsl.2016.06.012
- Torres, M. A., West, A. J., & Li, G. (2014). Sulphide oxidation and carbonate dissolution as a source of CO₂ over geological timescales. *Nature*, 507(7492), 346–349. https://doi.org/10.1038/nature13030
- Viviroli, D., Archer, D. R., Buytaert, W., Fowler, H. J., Greenwood, G. B., Hamlet, A. F., et al. (2011). Climate change and mountain water resources: Overview and recommendations for research, management and policy. *Hydrology and Earth System Sciences*, 15(2), 471–504. https://doi.org/10.5194/hess-15-471-2011
- Von Blanckenburg, F., Bouchez, J., Ibarra, D. E., & Maher, K. (2015). Stable runoff and weathering fluxes into the oceans over Quaternary climate cycles. *Nature Geoscience*, 8(7), 538–542. https://doi.org/10.1038/ngeo2452
- Walker, J. C., Hays, P. B., & Kasting, J. F. (1981). A negative feedback mechanism for the long term stabilization of Earth's surface temperature. Journal of Geophysical Research, 86(C10), 9776–9782. https://doi.org/10.1029/jc086ic10p09776
- Watson, A. J., & Lovelock, J. E. (1983). Biological homeostasis of the global environment: The parable of Daisyworld. *Tellus B: Chemical and Physical Meteorology*, 35(4), 284–289. https://doi.org/10.1111/j.1600-0889.1983.tb00031.x
- West, A. J. (2012). Thickness of the chemical weathering zone and implications for erosional and climatic drivers of weathering and for carbon-cycle feedbacks. *Geology*, 40(9), 811–814. https://doi.org/10.1130/g33041.1
- West, A. J., Galy, A., & Bickle, M. (2005). Tectonic and climatic controls on silicate weathering. Earth and Planetary Science Letters, 235(1–2), 211–228. https://doi.org/10.1016/j.epsl.2005.03.020
- Wickham, J., Stehman, S. V., Sorenson, D. G., Gass, L., & Dewitz, J. A. (2021). Thematic accuracy assessment of the NLCD 2016 land cover for the conterminous United States. *Remote Sensing of Environment*, 257, 112357. https://doi.org/10.1016/j.rse.2021.112357
- Wilson, F. H., Hults, C. P., Mull, C. G., & Karl, S. M. (2015). *Geologic map of Alaska*. U.S. Geological Survey. https://doi.org/10.3133/sim3340 Winnick, M. J., Carroll, R. W., Williams, K. H., Maxwell, R. M., Dong, W., & Maher, K. (2017). Snowmelt controls on concentration-discharge relationships and the balance of oxidative and acid-base weathering fluxes in an alpine catchment, East River, Colorado. *Water Resources Research*, 53(3), 2507–2523. https://doi.org/10.1002/2016wr019724
- Winnick, M. J., & Maher, K. (2018). Relationships between CO₂, thermodynamic limits on silicate weathering, and the strength of the silicate weathering feedback. *Earth and Planetary Science Letters*, 485, 111–120. https://doi.org/10.1016/j.epsl.2018.01.005

MUÑOZ ET AL. 23 of 24



Journal of Geophysical Research: Earth Surface

- 10.1029/2023JF007255
- Wojcik, R., Eichel, J., Bradley, J. A., & Benning, L. G. (2021). How allogenic factors affect succession in glacier forefields. *Earth-Science Reviews*, 218, 103642. https://doi.org/10.1016/j.earscirev.2021.103642
- Wymore, A. S., Brereton, R. L., Ibarra, D. E., Maher, K., & McDowell, W. H. (2017). Critical zone structure controls concentration-discharge relationships and solute generation in forested tropical montane watersheds. *Water Resources Research*, 53(7), 6279–6295. https://doi.org/10.1002/2016wr020016
- Wymore, A. S., Larsen, W., Kincaid, D. W., Underwood, K. L., Fazekas, H. M., McDowell, W. H., et al. (2023). Revisiting the origins of the power-law analysis for the assessment of concentration-discharge relationships. *Water Resources Research*, 59(8), e2023WR034910. https://doi.org/10.1029/2023wr034910
- Yamazaki, D., Ikeshima, D., Tawatari, R., Yamaguchi, T., O'Loughlin, F., Neal, J. C., et al. (2017). A high-accuracy map of global terrain elevations. Geophysical Research Letters, 44(11), 5844–5853. https://doi.org/10.1002/2017gl072874
- Zeebe, R. E., & Wolf-Gladrow, D. (2001). CO₂ in seawater: Equilibrium, kinetics, isotopes. Gulf Professional Publishing.
- Zemp, M., Frey, H., Gärtner-Roer, I., Nussbaumer, S. U., Hoelzle, M., Paul, F., et al. (2015). Historically unprecedented global glacier decline in the early 21st century. *Journal of Glaciology*, 61(228), 745–762. https://doi.org/10.3189/2015jog15j017

MUÑOZ ET AL. 24 of 24